The Plant Cell, Vol. 17, 182–203, January 2005, www.plantcell.org © 2004 American Society of Plant Biologists

Reverse Genetic Characterization of Cytosolic Acetyl-CoA Generation by ATP-Citrate Lyase in Arabidopsis [W]

Beth L. Fatland,[a,b] Basil J. Nikolau,[b] and Eve Syrkin Wurtele[a,1]

[a]Department of Genetics and Developmental and Cellular Biology, Iowa State University, Ames, Iowa 50011
[b]Department of Biochemistry, Biophysics and Molecular Biology, Iowa State University, Ames, Iowa 50011

Acetyl-CoA provides organisms with the chemical flexibility to biosynthesize a plethora of natural products that constitute much of the structural and functional diversity in nature. Recent studies have characterized a novel ATP-citrate lyase (ACL) in the cytosol of *Arabidopsis thaliana*. In this study, we report the use of antisense RNA technology to generate a series of Arabidopsis lines with a range of ACL activity. Plants with even moderately reduced ACL activity have a complex, bonsai phenotype, with miniaturized organs, smaller cells, aberrant plastid morphology, reduced cuticular wax deposition, and hyperaccumulation of starch, anthocyanin, and stress-related mRNAs in vegetative tissue. The degree of this phenotype correlates with the level of reduction in ACL activity. These data indicate that ACL is required for normal growth and development and that no other source of acetyl-CoA can compensate for ACL-derived acetyl-CoA. Exogenous malonate, which feeds into the carboxylation pathway of acetyl-CoA metabolism, chemically complements the morphological and chemical alterations associated with reduced ACL expression, indicating that the observed metabolic alterations are related to the carboxylation pathway of cytosolic acetyl-CoA metabolism. The observations that limiting the expression of the cytosolic enzyme ACL reduces the accumulation of cytosolic acetyl-CoA–derived metabolites and that these deficiencies can be alleviated by exogenous malonate indicate that ACL is a nonredundant source of cytosolic acetyl-CoA.

INTRODUCTION

Juxtaposed between anabolism and catabolism, acetyl-CoA is an intermediate common to a variety of metabolic processes that are distributed across at least five different subcellular compartments (Figure 1). In plastids, acetyl-CoA is the precursor for de novo fatty acid biosynthesis (Nikolau et al., 2003) and for the biosynthesis of glucosinylates (Falk et al., 2004). Mitochondrial acetyl-CoA is incorporated into the TCA cycle and used for the generation of ATP and the synthesis of amino acid carbon skeletons. In microbodies, acetyl-CoA is generated during fatty acid β-oxidation. In the nucleus, acetyl-CoA is the substrate for the acetylation of proteins, such as histones and transcription factors, and regulates their function in maintaining or altering chromosome structure and/or gene transcription (Choi et al., 2003; Sun et al., 2003).

In the cytosol, acetyl-CoA is required for the biosynthesis of a plethora of phytochemicals, many of which are important for plant growth, development, and responses to environmental cues (Schmid et al., 1990; Clouse, 2002; Souter et al., 2002). Cytosolic acetyl-CoA is metabolized via one of three mechanisms: carboxylation, condensation, or acetylation (Figure 1). Products of the carboxylation pathway include elongated fatty acids (which are used in the biosynthesis of some seed oils, some membrane phospholipids, the ceramide moiety of sphingolipids, the cuticle, cutin, and suberin), flavonoids, and malonyl derivatives (e.g., D-amino acids and malonylated flavonoids) and malonic acid (Hrazdina et al., 1978; Kolattukudy, 1980; Pollard and Stumpf, 1980; Stumpf and Burris, 1981; Hohl and Barz, 1995; Bao et al., 1998; Bohn et al., 2001; Sperling and Heinz, 2003). Condensation first forms acetoacetyl-CoA and subsequently leads to the biosynthesis of mevalonate-derived isoprenoids, such as sesquiterpenes, sterols, and brassinosteroids (Disch et al., 1998). Acetylation reactions occur in several subcellular compartments, and products include acetylated phenolics, alkaloids, isoprenoids, anthocyanins, and sugars (Pauly and Scheller, 2000; Bloor and Abrahams, 2002; Shalit et al., 2003; Whitaker and Stommel, 2003; Wiedenfeld et al., 2003).

Because acetyl-CoA is membrane impermeable (Brooks and Stumpf, 1966), acetyl-CoA biogenesis is thought to occur in each subcellular compartment where it is required (Liedvogel, 1986; Fatland et al., 2002; Schwender and Ohlrogge, 2002). This compartmentation and the multiple metabolic fates of acetyl-CoA have complicated the elucidation of acetyl-CoA's biogenesis (Mattoo and Modi, 1970; Murphy and Stumpf, 1981; Givan, 1983; Kaethner and ap Rees, 1985; Randall et al., 1989; Rangasamy and Ratledge, 2000). However, expanding genomic data (Wurtele et al., 1999; Ke et al., 2000; Behal et al., 2002; Fatland et al., 2002; Lin et al., 2003) in combination with metabolic flux analysis (Schwender et al., 2003) is facilitating the scrutiny of acetyl-CoA generation and metabolism.

Recently, ATP-citrate lyase (ACL) has been characterized in plants at the genomic level (Fatland et al., 2002). This enzyme

[1] To whom correspondence should be addressed. E-mail mash@iastate.edu; fax 515-294-1337.
The author responsible for distribution of materials integral to the findings presented in this article in accordance with the policy described in the Instructions for Authors (www.plantcell.org) is: Eve Syrkin Wurtele (mash@iastate.edu).
[W]Online version contains Web-only data.
Article, publication date, and citation information can be found at www.plantcell.org/cgi/doi/10.1105/tpc.104.026211.

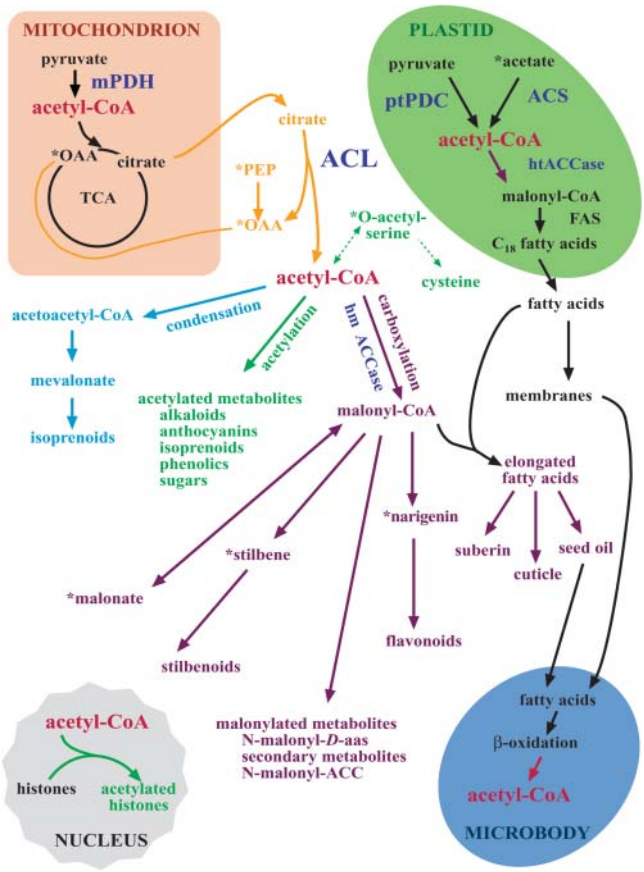

Figure 1. Subcellular Compartmentation of Acetyl-CoA Metabolism in Plants.

There are at least five distinct subcellular acetyl-CoA pools: cytosolic, mitochondrial, nuclear, plastidic, and peroxisomal. These pools are metabolized via the carboxylation (purple arrows), the condensation (blue arrows), or the acetylation pathways (green arrows) to generate a multitude of different metabolites. ACL acts on cytosolic citrate, generated by a postulated citrate shunt cycle (orange), to produce the cytosolic acetyl-CoA pool. Metabolites identified with an asterisk were tested for their ability to revert the antisense-*ACLA* phenotype. *N*-malonyl-ACC, *N*-malonyl-amino cyclopropane carboxylic acid.

catalyzes the ATP-dependant reaction of citrate and CoA to form acetyl-CoA and oxaloacetic acid. Plant ACL is a heterooctamer consisting of ACLA and ACLB subunits. In *Arabidopsis thaliana*, a small gene family encodes each subunit. The ACLA subunit is encoded by three genes (*ACLA-1*, At1g10670; *ACLA-2*, At1g60810; *ACLA-3*, At1g09430), and the ACLB subunit is encoded by two genes (*ACLB-1*, At3g06650; *ACLB-2*, At5g49460). Initial molecular characterizations of these genes have established that ACL is a cytosolic enzyme, implying that it generates a cytosolic pool of acetyl-CoA (Fatland et al., 2002).

To understand the significance of the ACL-derived acetyl-CoA pool in plant metabolism, growth, and development, plants with reduced ACL activity were generated and characterized. Such plants have a complex, altered phenotype and are specifically deficient in phytochemicals derived from cytosolic acetyl-CoA (e.g., cuticular waxes and seed coat pigments), indicating that ACL generates acetyl-CoA required for the production of these metabolites. Exogenous malonate, a compound that we hypothesize complements the carboxylation pathway of cytosolic acetyl-CoA metabolism, alleviates the ACL-deficient phenotype. Our findings indicate that an adequate ACL-generated cytosolic acetyl-CoA pool is essential for normal growth and development and that no other source of acetyl-CoA can compensate for deficiencies in this pool.

RESULTS

Antisense-*ACLA* Plants Express a Severely Altered and Complex Morphological Phenotype

To reduce ACL activity, the *ACLA-1* antisense RNA was expressed in Arabidopsis plants under the transcriptional control of the 35S promoter of *Cauliflower mosaic virus* (CaMV). Two hundred and twenty independently transformed plant lines were evaluated (Figure 2A). Fifty-seven of these were designated as expressing a mild phenotype, in that they diverged from normal growth only during reproductive development. The remaining 163 demonstrated different degrees of a striking dark-green bonsai phenotype (Figures 2A, 3A, and 3B), accentuated by the hyperaccumulation of purple pigment (Figure 3B). These latter plants were classified into four categories based upon their increasing morphological divergence from wild-type plants. These categories are termed moderate, severe, very severe, and lethal (Figure 2A).

During the vegetative stage of growth, the physical appearance of the phenotypically mild antisense-*ACLA* plants is similar to wild-type plants. Thus, their vegetative size, as measured by the fresh weight of the plant (Figure 2B), the diameter of the fully expanded rosette (Figure 2C), and the height of the mature bolt (Figure 2D) were similar to wild-type plants. However, features that distinguish these mild-phenotype plants from wild-type plants become apparent in the reproductive organs. Specifically, the number of reproductive structures per plant is reduced (Figure 2E), a larger proportion of siliques are aberrant (Figure 2E), and seed yield (Figure 2F) and germination in moderate-phenotype plants (Figure 2G) are reduced (germination of seeds from the phenotypically severe mutant is not reduced, probably because the aberrant seeds were so small and undeveloped that they were not collected in the harvest). Additionally, the antisense-*ACLA* plants senesce 7 to 35 d after wild-type plants (Figure 2H).

Antisense-*ACLA* plants that express moderate, severe, very severe, and lethal phenotypes are considerably smaller in size, as measured by the weight of the fully expanded plant (Figure 2B), the diameter of the rosette (Figure 2C), and the height of the bolt (Figure 2D). These parameters diminish as the phenotype intensifies from moderate to lethal. In addition, these plants show a greater mortality rate than wild-type plants in the first 3 to 4 weeks of growth (data not shown). Another change associated with this group of antisense plants is a large reduction in fecundity as compared with wild-type and mild-phenotype plants. Thus, the total number of reproductive entities (flower buds, flowers, and siliques) and the proportion of normal siliques

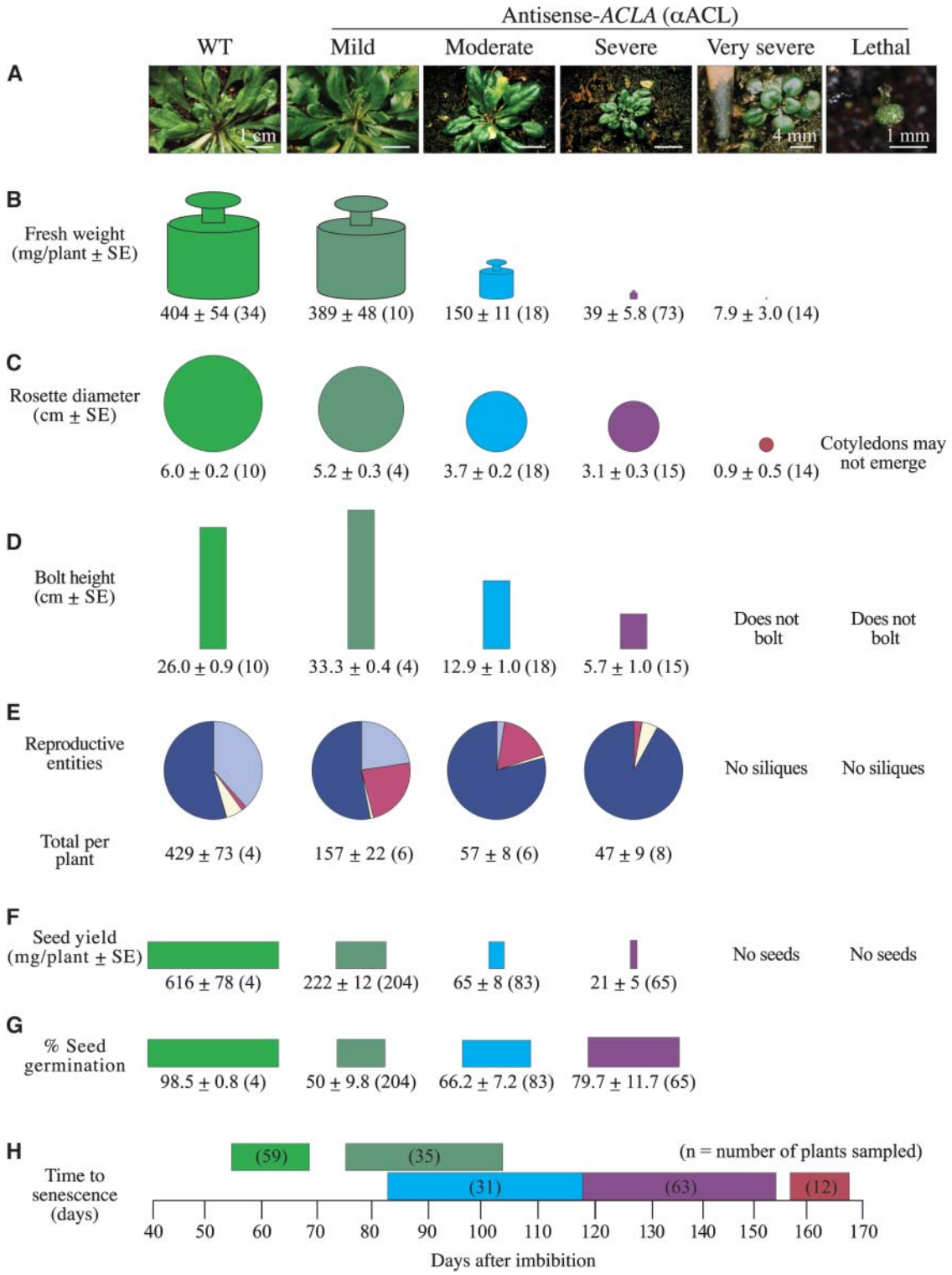

Figure 2. Antisense-*ACLA* Plants Are Reduced in Size and Altered in Development.

Graphic representation of the physical traits of wild-type and antisense-*ACLA* (αACL) associated phenotypes categorized as either mild, moderate, severe, very severe, or lethal.

(A) Representative wild-type and αACL plants at 78 DAI, presenting different phenotype classes.

(B) Fresh weight of 78-DAI plants.

incrementally decrease as the phenotype intensifies. In parallel, seed yield and seed germination decrease and plants display increasingly delayed senescence (Figures 2F and 2H).

Moderate and severe phenotypic classes are differentiated from each other by quantitative changes in the traits described above. However, the differences among severe, very severe, and lethal categories are qualitative changes in select traits. Namely, whereas plants in the severe category bolt and thus produce seeds, those in the very severe category do not bolt and hence cannot produce seeds (Figures 2D and 2F). Failure to survive past the cotyledon stage characterizes plants in the lethal category: seeds in this category either fail to germinate or germinate but die shortly after radicle or cotyledon emergence (Figures 2A, 3C, and 3D).

The integration of five phenomena contributes to the complex phenotype associated with the antisense-*ACLA* plants. These are changes in phytomer size, growth rate, timing of developmental transitions, apical dominance, and accumulation of metabolites. First, the diminutive appearance of antisense-*ACLA* plants is attributable to a proportional reduction in the overall size of the shoot's phytomers (Figure 2A). This reduction becomes apparent early in the development of seedlings (Figure 3E versus 3F) and affects the first true leaves, the petioles (Figure 3E), and the primary roots (Figure 3G), which are all shorter than the wild type (Figures 3E and 3G). The reduction in the size of the phytomers extends throughout the life cycle of the plant and affects the size of all leaves (Figure 3J), the inflorescence stem (Figure 3K), and reproductive structures (Figures 3L to 3N). Petals, which normally extend beyond sepals of mature flowers, are barely visible in antisense-*ACLA* plants (Figures 3L and 3M). The anthers and stigmas are shorter than normal, and siliques are shorter, often curled, and unevenly expanded (Figures 2E and 3M).

Second, the miniaturization of antisense-*ACLA* plants is because of a reduction in the growth rate of both rosettes (Figure 4A) and bolts (Figure 4B). For example, over the 12-d period, between 20 and 32 d after imbibition (DAI), the rate of rosette expansion of antisense-*ACLA* plants with moderate and severe phenotypes is 37 and 16% of wild-type plants, respectively (Figure 4A). Similarly, the rate of growth of the inflorescence stem is reduced in antisense-*ACLA* plants with a moderate phenotype and even more so in plants with a severe phenotype (Figure 4B).

Third, multiple developmental transitions are either delayed or fail to occur in antisense-*ACLA* plants. One of these is bolting; whereas most of the wild-type plants have bolted by 24 DAI, <70% of the antisense plants with a moderate or severe phenotype have bolted at this stage (Figure 4C). Furthermore, plants with a very severe phenotype do not bolt even after 126 d. Flower opening is also delayed; at the height of flowering, when only 48% of the reproductive units on wild-type plants exist as closed flower buds, 53, 80, and 92% of these structures are still at the closed flower bud stage on antisense-*ACLA* plants expressing mild, moderate, and severe phenotypes, respectively (Figure 2E). When siliques are produced on antisense-*ACLA* plants, they often open prematurely and release immature seeds (Figure 3O). Of the seeds that are harvestable, many contain embryos that are delayed in development. For example, seeds containing embryos at the globular, torpedo, young walking-stick stage of development are common (Figure 3S). Such seeds do not germinate successfully, although some steps of seed germination may occur (e.g., seed coat splitting and partial emergence of the radicle). The proportion of aberrant seeds increases as the antisense phenotype intensifies, which explains the observed reduction in the rate of seed germination (Figure 2G). In addition, because the embryo within such seeds is not fully mature, these seeds are aberrantly shaped and/or are smaller in size (Figures 3P to 3Q). The developmental transition into senescence is also affected by the antisense-*ACLA* transgene. Thus, antisense-*ACLA* plants remain green longer and senesce at later stages than wild-type plants (Figures 2H and 3A). For example, antisense plants showing a severe and very severe phenotype remain suspended in a diminutive state with a characteristic dark green color for up to 154 d and at least 160 d, respectively (Figure 2H).

Fourth, antisense-*ACLA* plants have reduced apical dominance. This is apparent in roots of young seedlings and in inflorescence stems. Thus, the primary roots of young seedlings are shorter, whereas secondary roots are longer (Figure 3H versus 3I). Additionally, secondary inflorescence stems are initiated in rapid succession, resulting in plants with a shrub-like appearance (Figures 3A and 3B).

Finally, the visual appearance of antisense-*ACLA* plants is indicative of changes in the underlying metabolites. Most apparently, these plants are highly pigmented (Figures 3J and 3V), but seed coat pigmentation is reduced (Figure 3P) and is labile upon treatment with perchloric acid during seed sterilization (cf. Figure 3T versus 3U).

The Altered Phenotype Cosegregates with the Antisense-*ACLA-1* Transgene

To determine whether the phenotypic characteristics (described above) are linked to the 35S:antisense *ACLA-1* transgene, PCR was used to monitor the inheritance of the transgene. Seeds from a single heterozygous transgenic T2 plant were sown on soil. For each of the resulting 84 T3 plants, the phenotype was recorded

Figure 2. (continued).

(C) Rosette diameter of 78-DAI plants.

(D) Bolt height at 78 DAI.

(E) Total number and proportion of reproductive entities per plant at 42 DAI: normal siliques (g), curled siliques (g), short siliques (g), and flower buds (g).

(F) Seed yield per plant.

(G) Seed germination rates.

(H) Time to senescence: senescence is defined as the age at which the majority of siliques are dry and ready to be harvested. Each numerical parameter represents the average ± SE of *n* replicates (*n* is given in parentheses).

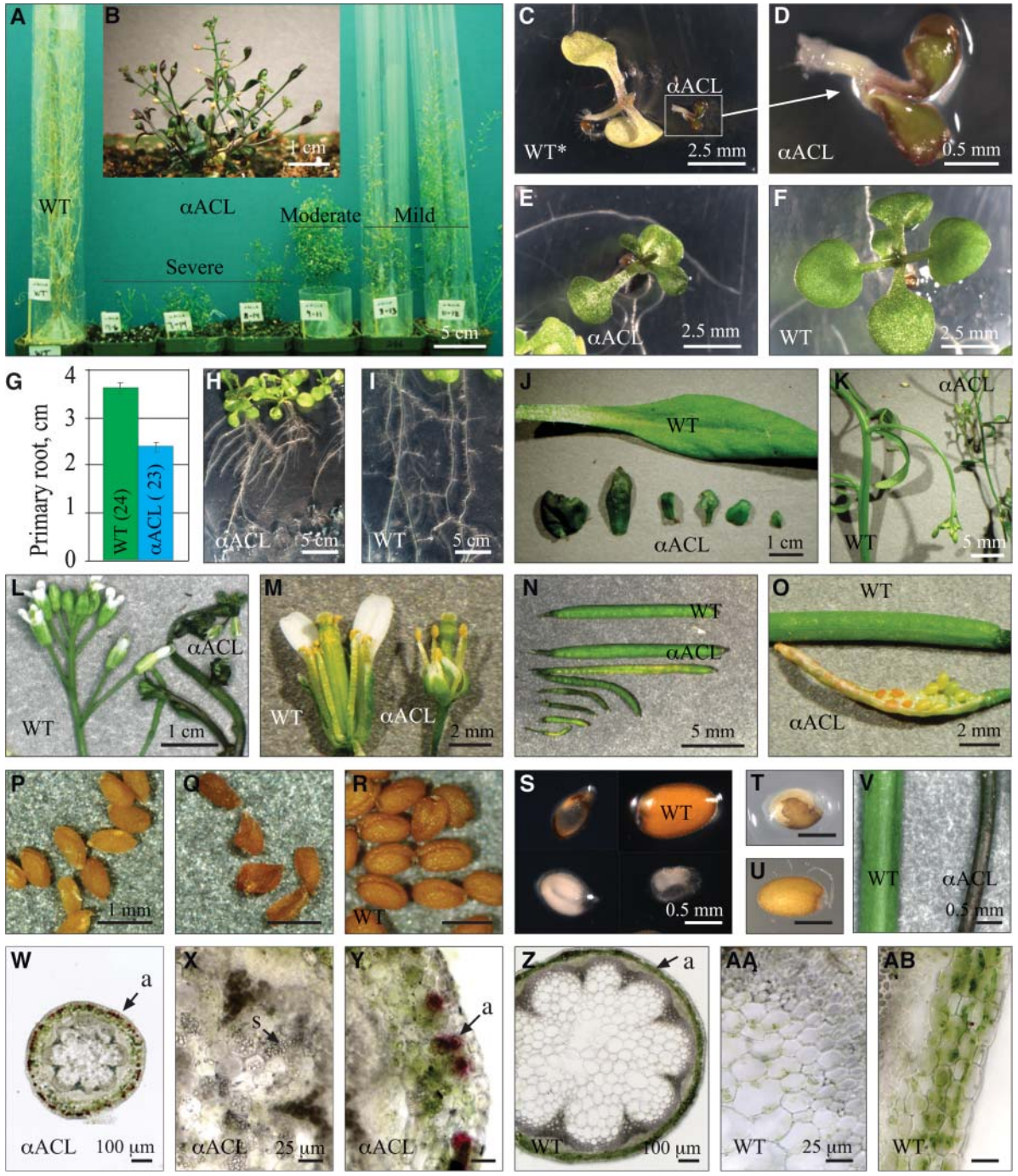

Figure 3. Antisense-*ACLA* Plants Have Complex, Aberrant Phenotypes.

(A) Representative wild-type and antisense-*ACLA* (αACL) plants of severe, moderate, and mild phenotypes at 80 DAI.
(B) αACL plant at 80 DAI, demonstrating the severe phenotype.
(C) to **(F)** Wild-type and αACL seedlings at 9 DAI germinated either in the presence (**[C]** to **[E]**) or absence **(F)** of kanamycin. In **(C)**, the asterisk indicates that the wild-type seedling is chlorotic as a result of the presence of kanamycin in the media; the plant with the very severe phenotype is magnified in **(D)**.
(G) Primary root length of wild-type and αACL seedlings at 7 DAI; n = number of plants measured.
(H) and **(I)** Roots of wild-type and αACL seedlings at 9 DAI.
(J) Leaves from 47-DAI wild-type plants and 85-DAI αACL plants with severe phenotype.
(K) Inflorescence stems from wild-type and αACL plants with a moderate phenotype.
(L) Shoot apical meristem from a wild-type and an αACL plant with a severe phenotype.

and PCR was conducted using transgene-specific primers. Sixty-five of 84 siblings possessed the characteristic phenotype and primers amplified a transgene-specific PCR product of the expected size from each of these plants, indicating the presence of the transgene. The other 19 plants were PCR negative and had a wild-type phenotype. The χ^2 test (data not shown) confirms the transgene segregates at a ratio of 3:1 and thus is inherited as a single locus. These data, in combination with the fact that 163 of 220 independent transgenic lines have the same phenotype, indicate that this characteristic phenotype is because of the presence of the 35S:antisense *ACLA-1* transgene.

Both ACLA and ACLB Expression Are Reduced in Antisense-*ACLA* Plants

The level of ACLA and ACLB proteins was determined in shoots from four independent antisense-*ACLA* lines varying in phenotype severity. Protein gel blot analysis indicates that the abundance of the ACLA protein in antisense-*ACLA* plants is reduced (Figure 5A). In antisense-*ACLA* plants with a severe phenotype, the accumulation of ACLA protein is reduced by ~45% (Figure 5D), but in antisense-*ACLA* plants that show a mild phenotype, the level of ACLA protein is not significantly different from that found in wild-type plants (Figure 5D).

To determine the effect of the antisense-*ACLA* transgene on ACL activity, a spectrophotometric technique (Fatland et al., 2002) was used to assay this enzyme in extracts from antisense-*ACLA* plants. Whereas plants with the mild phenotype show no quantifiable decrease in ACL activity as compared with wild-type plants, ACL activity in plants with moderate and severe phenotypes is reduced to ~50 and 35% of wild-type levels (Figure 5E). This reduction in ACL activity is maintained throughout the growth of these plants (Figure 5F). Thus, the intensity of the antisense-*ACLA* phenotype is correlated with a reduction in ACL activity. As would be expected, the reduction in ACL activity is proportional to the reduction in the accumulation of the ACLA subunit.

To investigate the possibility of cross talk between ACLA and ACLB expression, the levels of ACLB were immunologically determined in plants with reduced levels of the ACLA subunit. There is a near-identical reduction in both ACLA and ACLB proteins in these antisense *ACLA* plants (Figures 5B and 5D), indicating that there is communication between the expression of the ACLA and ACLB subunits.

Reduction in ACL Expression Impedes Cellular Expansion

The reduction in leaf size in the antisense-*ACLA* plants could be because of a decrease in cell number or cell size, indicating impeded cell division or expansion, respectively. To distinguish between these possibilities, and to assess tissue organization, leaves from wild-type and antisense-*ACLA* plants were examined microscopically.

Tissue organization in leaves from antisense-*ACLA* (Figure 6A) and wild-type plants (Figure 6B) is similar, with clearly delineated palisade and spongy mesophyll and epidermal layers. Despite this normal tissue organization, overall cell size is conspicuously reduced in antisense-*ACLA* plants (Figure 6A versus 6B, and 6C versus 6D). This reduction in cell size occurs to a greater extent along the cell's width as compared with the cell's length (Figure 6E). The width of epidermal, palisade, and spongy mesophyll cells are 77, 61, and 88% that of wild-type cells, respectively, whereas only the lengths of spongy mesophyll cells and epidermal cells are slightly reduced. This reduction in cell size, as well as a concomitant reduction in apoplastic space, leads to a more compact, thinner leaf lamina (Figure 6C versus 6D). Hence, decreased ACL expression does not alter laminar topology but inhibits cellular growth and thus organ expansion.

Reduction in ACL Expression Alters Cellular Ultrastructure

Comparison of leaves from wild-type and antisense-*ACLA* plants using light microscopy and transmission electron microscopy reveals an altered ultrastructure. The most striking difference is the prominent oblong material that packs the large numbers of plastids within the mesophyll cells of antisense-*ACLA* plants (Figures 6A and 6C). Furthermore, the vacuoles are smaller in antisense-*ACLA* plants, and the cytoplasm accounts for a larger proportion of the cell's volume (Figure 6H versus 6K). In addition, small spherical bodies (500 ± 30 nm in diameter) accumulate in mesophyll cells (e.g., Figures 6F and 6I); these are absent from comparable wild-type cells (Figures 6J and 6L). These bodies appear to be bound by a single membrane and are granular in appearance, but their composition is unknown. The mitochondria and peroxisomes in cells of antisense-*ACLA* plants appear normal.

As with mesophyll cells, the plastids of epidermal cells of antisense-*ACLA* plants accumulate dense crystalline material (Figures 6F to 6I); this material is not present in the plastids of

Figure 3. (continued).

(M) Flowers from a wild-type plant and an αACL plant.
(N) A representative wild-type silique and siliques from αACL plants with a variety of phenotypes.
(O) Siliques from a wild-type and an αACL plant showing premature seed release.
(P) and **(Q)** Representative seeds from αACL plants.
(R) Representative wild-type seeds.
(S) Representative seeds from αACL plants showing a variety of phenotypes.
(T) The seed coat pigmentation of αACL seeds is lost upon sterilization with bleach.
(U) Wild-type seeds retain color during sterilization with bleach.
(V) Inflorescence stems from wild-type and αACL plants.
(W) to **(AB)** Micrographs of fresh vibratome sections from the base of the primary inflorescence stems of αACL plants (**[W]** to **[Y]**) and wild-type plants (**[Z]** to **[AB]**). a, anthocyanin; s, starch.

wild-type epidermis (Figures 6J to 6L). This layer of cells also accumulates elevated levels of round purple bodies (~3.5 ± 0.2 μm in size), presumed to be anthocyanin-containing vacuoles (Figures 6C and 6F). These differences in cellular composition and ultrastructure indicate that reduction in ACL activity interrupts normal processes of primary metabolism and cell growth.

Reduction in ACL Expression Alters Plastid Ultrastructure and Leads to the Hyperaccumulation of Starch

The plastids of leaves from antisense-*ACLA* plants (Figure 6I) are distinct from those of wild-type plants (Figure 6L), having fewer thylakoid membranes, smaller plastoglobuli, and lacking highly

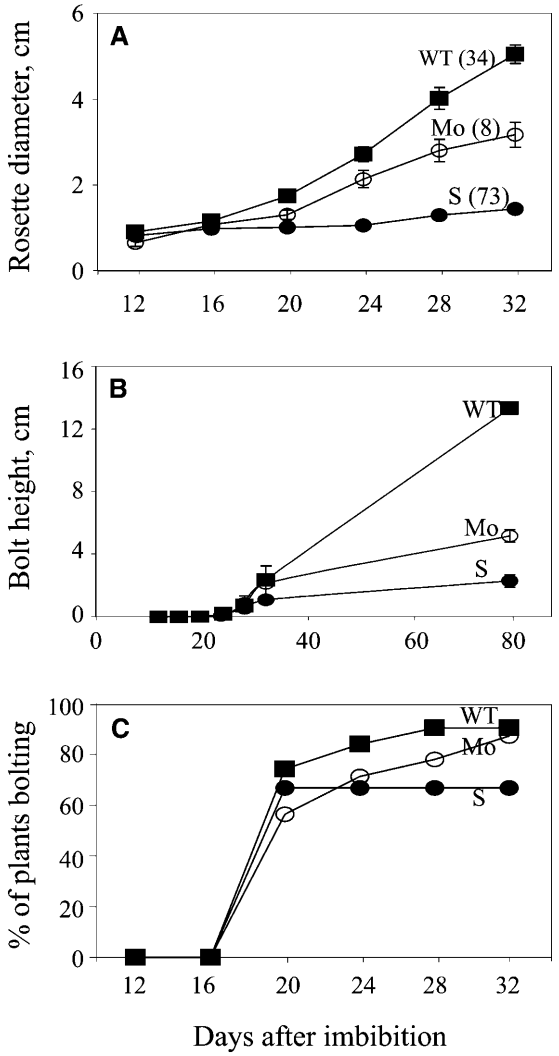

Figure 4. Antisense-*ACLA* Plants Grow at Slower Rates.

Wild-type and antisense-*ACLA* plants with a moderate (Mo) or severe (S) phenotype were grown in soil, and at the indicated times, the rosette diameter **(A)**, the height of the bolt **(B)**, and the proportion of plants that had bolted **(C)** were determined. Numbers in parentheses represent the number of plants measured. Bars represent ±SE.

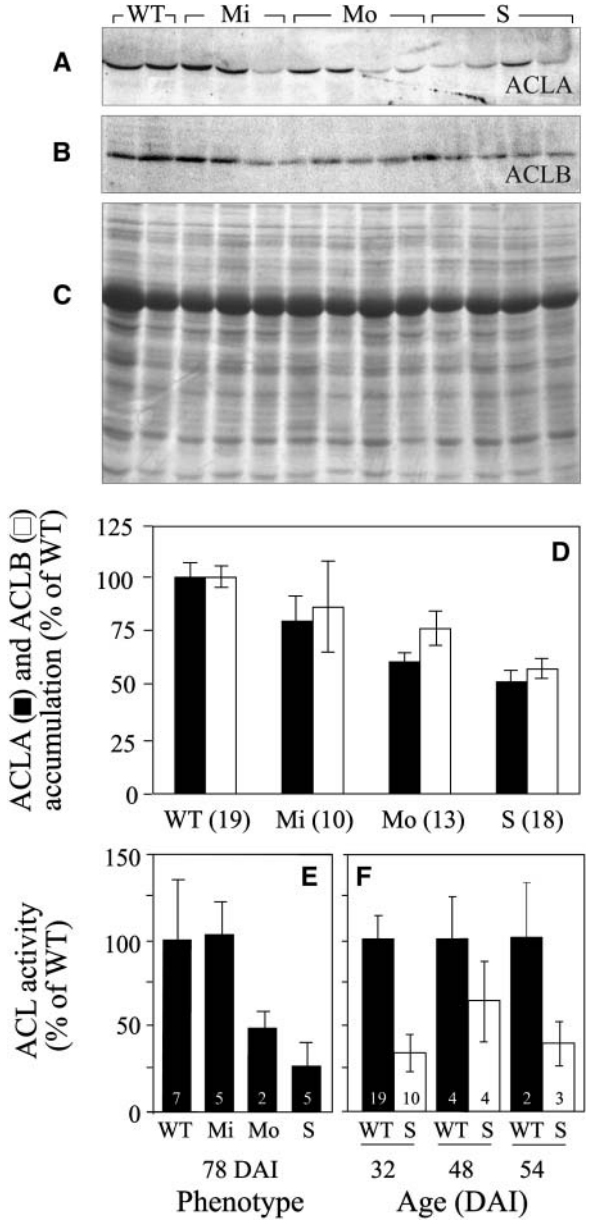

Figure 5. ACL Expression Is Reduced in Antisense-*ACLA* Plants That Show an Altered Growth Phenotype.

(A) to **(C)** ACL expression was determined in wild-type and antisense-*ACLA* plants showing a mild (Mi), moderate (Mo), or severe (S) phenotype. Protein extracts (100 μg protein/lane) from plants at 40 DAI were separated by SDS-PAGE. Resulting gels were either subjected to protein gel blotting and ACL subunits were immunodetected with ACLA antisera **(A)** and ACLB antisera **(B)** or stained with Coomassie blue **(C)**.

(D) The intensity of the immunodetected ACLA and ACLB proteins was quantified with a PhosphorImager and normalized relative to wild-type levels.

(E) and **(F)** ACL specific activity in protein extracts from plants of 78 DAI **(E)** or from plants at the indicated age (<wild type; <αACL of severe phenotype) **(F)**. Number of plants analyzed is represented in parentheses **(D)** or on bars (**[E]** and **[F]**). Bars represent ±SE.

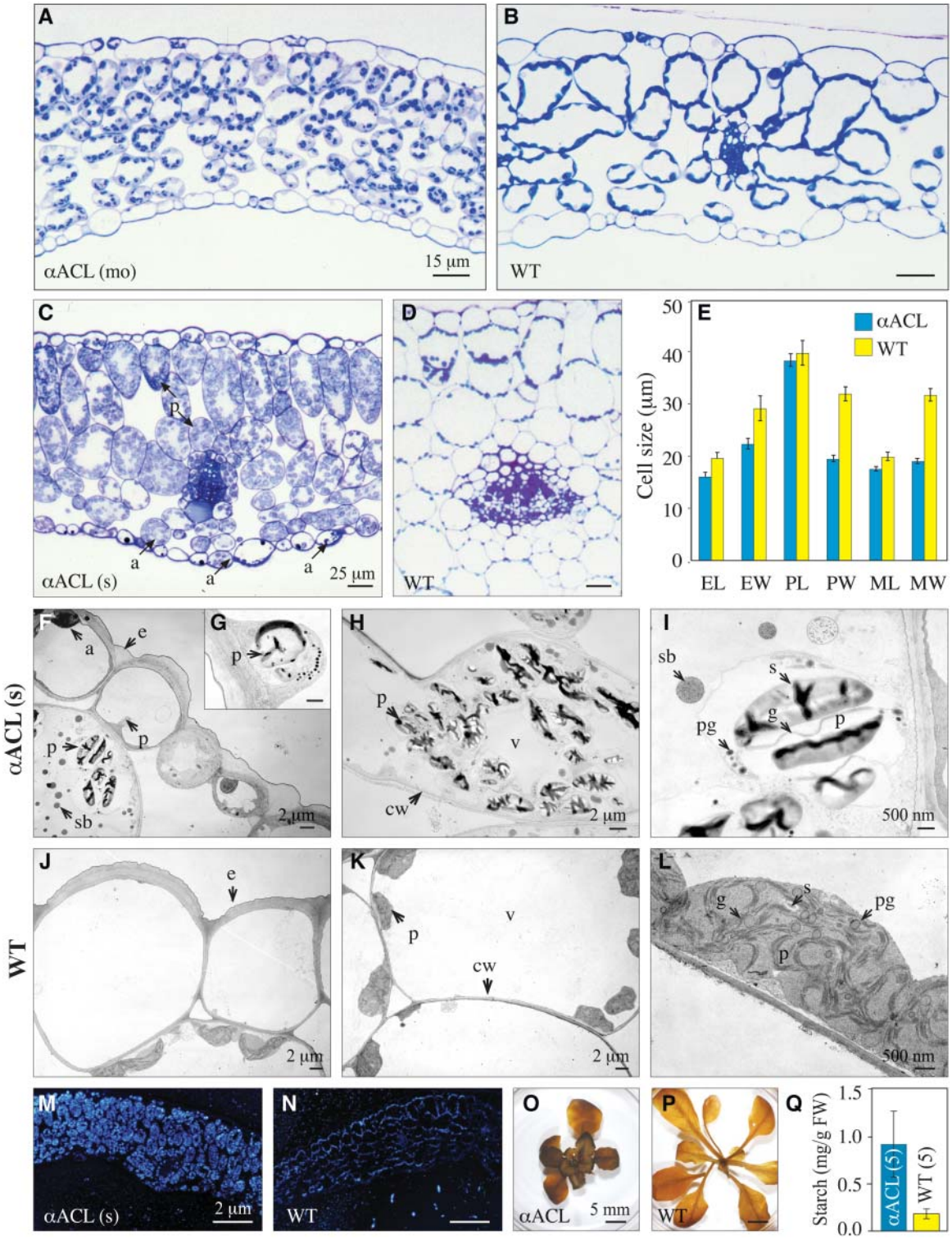

Figure 6. Reduction in ACL Expression Impedes Cellular Expansion, Alters Cellular Ultrastructure, and Leads to the Hyperaccumulation of Starch.

(A) to **(D)** Micrographs of midsections of fully expanded leaves from wild-type and antisense-*ACLA* (αACL) plants; the phenotypic category of each αACL plant is indicated. Four leaves from two independent transgenic lines were examined.

(E) Dimensions (length, L; width, W) of epidermal (E), palisade (P), and spongy mesophyll (M) cells of αACL and wild-type leaves at 26 DAI. For each genotype, dimensions were determined from midleaf cross sections taken from four separate plants. Thirty-two to 214 cells were measured for each category. SE is indicated.

stacked grana. Additionally, virtually all of these plastids contain prominent oblong granules (Figure 6H). Plastids within the pith of inflorescence stems of antisense-*ACLA* plants (86 DAI) (Figure 3X) also accumulate similar granules.

The chemical nature of these granules is indicated by their location within plastids and by the fact that they share characteristics with wild-type starch grains (Figure 6L). Namely, they have an ovoid shape, they are nonosmiophilic (osmium does not generally stain carbohydrates; Hayat, 2000), and under the electron microscope they show repeating electron-dense regions, implying a crystalline structure (Figure 6I). These characteristics indicate that these large particles are starch granules.

Histochemical methods were used to confirm this assessment. Sections from leaves of antisense-*ACLA* (as in Figure 6C) and wild-type plants (as in Figure 6D) were processed through the Thiery reaction (modified PAS-Schiff reaction). This reaction detects vicinal diols, functional groups that are prevalent in polysaccharides (Hall, 1978). The Thiery reaction stained the granules that accumulate in leaves from antisense-*ACLA* plants (Figure 6M). Moreover, this staining is more intense than in the wild-type plants (Figure 6N). Antisense-*ACLA* seedlings also stain more intensely with potassium iodide (IKI) (Figure 6O) than wild-type plants (Figure 6P). In toto, ultrastructural observations, in conjunction with the positive Thiery and IKI staining, are consistent with the granules being starch.

To measure starch content, water-insoluble polysaccharides were extracted from rosettes of antisense-*ACLA* and wild-type plants and assessed using an enzymatic starch assay (Keppler and Decker, 1974). Starch concentration in the antisense-*ACLA* plants is four times higher than in wild-type plants (Figure 6Q). This increased accumulation of starch indicates that in response to the reduction in ACL expression, there are significant changes in flux through primary metabolic pathways.

Reduction in ACL Expression Leads to Cell-Specific Changes in Pigments

To determine if the darker pigmentation of antisense-*ACLA* plants is because of the accumulation of anthocyanin, chlorophylls, or carotenoids, the absorbance of alcoholic extracts (Rabino and Mancinelli, 1986; Lichtenthaler, 1987) was used to calculate the concentration of these pigments (Figure 7). The concentration of chlorophylls and carotenoids is approximately two times higher in rosettes of antisense-*ACLA* plants as compared with wild-type plants (Figure 7A), and anthocyanin concentration is elevated approximately fourfold (Figure 7B). These results indicate that the enhanced coloration observed in antisense-*ACLA* plants is because of increases in these pigments, particularly the accumulation of anthocyanins.

This trend is visually reiterated by the enhanced accumulation of anthocyanin-containing vacuoles in the epidermis of leaves from antisense-*ACLA* plants (Figure 6C). Such red pigment is even more prevalent in the inflorescence stems of antisense-*ACLA* plants (Figures 3W and 3Y), where bright red–pigmented vacuoles fill almost the entire volume of the subepidermal cells. These pigmented vacuoles are much less common in wild-type stems (Figures 3Z and 3AB) and, if present, are much smaller than those found in antisense-*ACLA* plants.

In contrast with the hyperaccumulation of pigments in vegetative organs, seeds hypoaccumulate these molecules. Flavonoids are prevalent in Arabidopsis seeds as both free anthocyanins (Shirley, 1998) and as phlobaphen polymers; the latter forms the major component of the testa (Shirley et al., 1995; Stafford, 1995). Each individual antisense-*ACLA* plant produces seeds with a variety of pigmentation phenotypes ranging from lighter colored seeds to transparent seed coats (Figures 3P, 3Q, 3S, and 3T). Anthocyanin concentration within such a mixed seed population is ~60% of wild-type levels (Figure 7B). Thus, the reduction in seed color is attributable in part to a reduction in anthocyanins. In those seeds with a completely transparent seed coat, both phlobaphen and anthocyanins must be absent or highly reduced (Figure 3S).

Reduction in ACL Expression Alters Seed Fatty Acid Accumulation without Affecting Fatty Acid Composition

Seed lipids of Arabidopsis require cytosolic acetyl-CoA for the elongation of C18 fatty acids to C20 to C24 fatty acids (James and Dooner, 1991). Furthermore, during seed development, ACL mRNAs accumulate in the embryo and other parts of the seeds (Fatland et al., 2002). To determine if a reduction in ACL activity affects the fatty acids of seeds, lipids were extracted and fatty acids were analyzed via gas chromatography–mass spectrometry (GC-MS) (Figure 8). Lipid-associated fatty acids are reduced by 18 to 36% in seeds from three independent antisense-*ACLA* plant lines expressing a moderate phenotype (Figure 8A). However, the proportions of the individual fatty acids remain similar to those of wild-type plants (Figure 8B). The reduction in fatty acid concentration in the antisense-*ACLA* seeds probably reflects the fact that a portion of the seeds assayed contained abnormal embryos. The observation that the fatty acids in seeds from antisense-*ACLA* plants were not altered in composition is somewhat surprising. But given the low efficiency of expression of the 35S CaMV promoter during embryo expansion (Eccleston and

Figure 6. (continued).

(F) to **(L)** Electron micrographs of cells from leaves of αACL plants with a severe phenotype and wild-type plants at 54 DAI; four leaves from two plants were examined.

(F) and **(J)** Epidermal cells.

(H), **(I)**, **(K)**, and **(L)** Mesophyll cells.

(M) and **(N)** Phase contrast micrographs of Thiery reaction–stained leaf cross sections from αACL and wild-type plants.

(O) and **(P)** IKI-stained αACL and wild-type seedlings.

(Q) Starch accumulation in αACL and wild-type seedlings. Number of plants analyzed is represented in parentheses.

a, anthocyanin; cw, cell wall; e, epidermis; g, grana; p, plastid; pg, plastoglobuli; s, starch grain; sb, spherical body; v, vacuole.

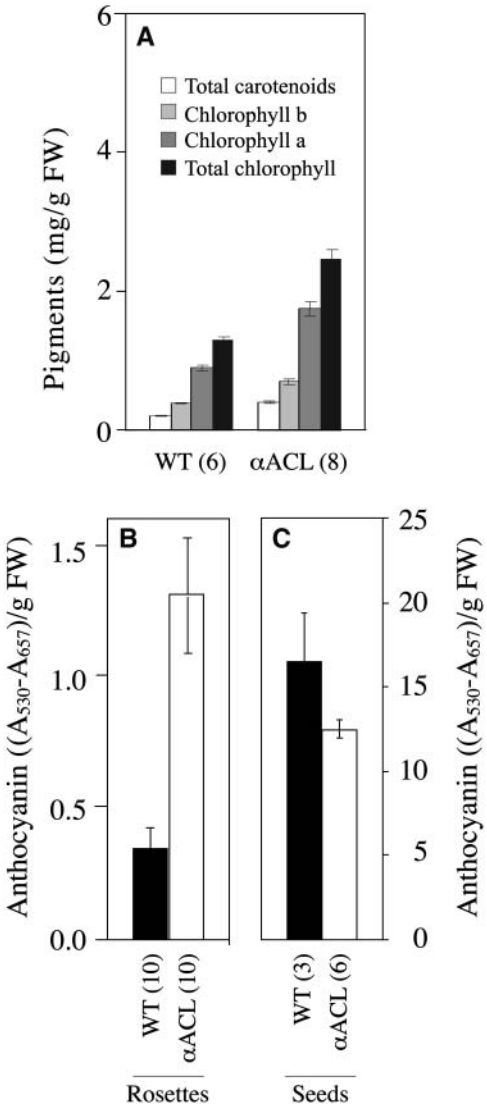

Figure 7. Antisense-*ACLA* Plants Express Altered Pigment Levels.

(A) Concentration of total carotenoids (white bars), chlorophyll *b* (light-gray bars), chlorophyll *a* (dark-gray bars), and total chlorophyll (black bars) in extracts of rosettes from 63-d-old plants. FW, fresh weight.
(B) and **(C)** Anthocyanin concentration in extracts from rosettes of 63-d-old plants **(B)** and seeds **(C)**. Number of samples assayed is represented in parentheses. Bars represent ±SE.

Ohlrogge, 1998; Desfeux et al., 2000), it may be an indication that the antisense-*ACLA* RNA was not effective in reducing ACL expression in developing embryos.

Reduction in ACL Expression Decreases Accumulation of Epicuticular and Cuticular Waxes

In epidermal cells, C18 fatty acids are elongated with carbon derived from cytosolic acetyl-CoA to generate the very long chain fatty acid precursors of cuticular waxes (Post-Beittenmiller, 1996). To investigate the affect of the antisense-*ACLA* transgene on cuticular waxes, a combination of microscopic and GC-MS analyses were used. An increase in inflorescence stem surface shine, which typically indicates a reduction in epicuticular waxes (Koorneef et al., 1989), is apparent in antisense-*ACLA* plants with moderate and severe phenotypes (data not shown). Scanning electron microscopy confirms that stems from antisense-*ACLA* plants (Figures 9A and 9B) have reduced epicuticular wax crystalloids when compared with wild-type specimens (Figure 9C). The degree of reduction varies along each stem, from the complete absence of crystalloids to a moderate crystalloid density, creating a patchy appearance (Figure 9B). The alteration in crystalloid density is accompanied by a subtle alteration in wax crystalloid morphology. As previously reported (Hannoufa et al., 1993), wax crystalloids on wild-type Arabidopsis inflorescences have a tube-and-plate morphology (Figure 9C). However, wax crystalloids, when they occur on antisense-*ACLA* stems, are smaller and have fibrous-shaped tubes and irregular plates (Figure 9B). This change in shape probably reflects an alteration in composition of cuticular wax.

GC-MS analysis was used to quantify the compositional changes in cuticular waxes associated with the antisense-*ACLA* plants. Cuticular wax loads from the inflorescence stems of antisense-*ACLA* plants with a severe phenotype are 72% less than that of wild-type inflorescence stems (Figure 9D). The antisense-*ACLA* plants had a significant reduction in four of the major constituents of cuticular waxes (C_{29} alkane, C_{26} and C_{28} primary alcohols, and C_{29} secondary alcohol). Additional reductions in the minor acyl-derived constituents and the triterpene, β-amyrin, occur (Figure 9E). These alterations support the hypothesis that ACL plays a role in cytosolic acetyl-CoA generation required for synthesis of cuticular waxes.

Exogenous Malonate Chemically Complements the Morphological and Chemical Phenotype Associated with Reduced ACL Expression

To test the hypothesis that antisense-*ACLA* plants are lacking one or more acetyl-CoA–derived compounds, plants were treated with a variety of metabolites known to require cytosolic acetyl-CoA for their production or with metabolites that can supplement the production of these compounds by alternative metabolism. Metabolites that were tested include acetate, malonate, naringenin, quercetin, *O*-acetyl-Ser, amino acids, oxaloacetate, phosphoenolpyruvate, and stilbene (Figure 1).

Of these treatments, only the application of malonate induced a striking reversion of the phenotype in the antisense-*ACLA* plants to a near wild-type appearance (Figure 10). Malonate-treated antisense-*ACLA* plants have larger rosettes than water-treated antisense-*ACLA* controls (Figures 10A and 10B). In parallel, malonate treatment of antisense-*ACLA* plants reduces pigmentation, resulting in plants that resemble wild-type plants (Figures 10C to 10E versus 10F). Accumulation of anthocyanin in antisense-*ACLA* plants is reduced by the malonate treatment to one-third the level of that in water-treated antisense-*ACLA* plants (Figures 10C and 10D). Malonate treatment has no detectable effect on the growth or appearance of wild-type plants (Figures 10A to 10F).

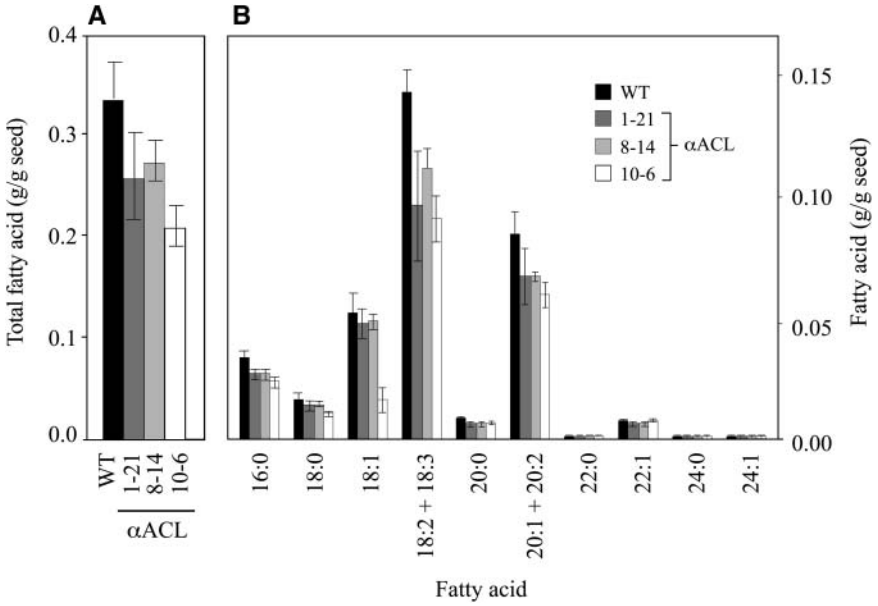

Figure 8. Seeds of Antisense-*ACLA* Plants Accumulate Lower Levels of Fatty Acids, but the Fatty Acid Profiles Are Unaltered.

Total fatty acid content **(A)** and levels of individual fatty acids **(B)** in populations of 100 seeds from wild-type and three independent antisense-*ACLA* (αACL) plant lines (1-21, 8-14, and 10-6). Average data ± SE from three replicates.

The malonate-induced enlargement of the antisense-*ACLA* leaves appears to be because of an increase in cell size (Figure 10G, two panels on right); whereas cells of the antisense leaves are small and cytoplasmically dense, treatment with malonate expands them to near wild-type size (Figure 10G). Interestingly, the widths of epidermal, palisade, and mesophyll cells increase to a greater extent than the lengths of these cells (Figure 10I). In parallel, there is an associated increase in the size of the vacuole and a reduction in the size of the plastids (Figure 10G).

Malonate treatment reduces the starch content of the antisense-*ACLA* plants, as determined by IKI staining of rosettes (Figure 10H) and by enzymatic analysis of starch content of the tissue (Figure 10J). Specifically, malonate treatment decreases starch content from 1.2 mg starch/g to 0.5 mg starch/g in the antisense plants, but this treatment does not alter starch concentration in wild-type plants (Figure 10J).

Malonate treatment of antisense-*ACLA* plants restores accumulation of epicuticular crystalloids and cuticular waxes to near wild-type levels. The epidermal surfaces of the upper, newly expanded regions (Figure 11A) of the stem from water- and malonate-treated antisense-*ACLA* plants are strikingly different; those treated with malonate have recovered the accumulation of epicuticular crystalloids (Figure 11A), whereas these structures are absent from the surfaces of the water-treated plants (Figure 11A). By contrast, stem sections that had already expanded before treatment with malonate were not affected (Figure 11B). A difference in crystalloid density is not apparent in wild-type plants after malonate treatment (Figure 11A versus 11B).

The restoration of cuticular wax accumulation was confirmed by quantification via GC-MS analysis. The quantity of cuticular wax on antisense-*ACLA* stems increases upon malonate treatment to levels similar to those found in wild-type plants (Figure 11C). Cuticular wax composition is also reverted to resemble wild-type composition, with the exception of the C_{26} constituents, which increase to higher than sixfold that of wild-type levels (Figure 11D). In combination, these results indicate that exogenous malonate alleviates disturbances caused by the reduction of ACL expression.

cDNA Microarrays Reveal Changes in mRNA Accumulation in Antisense-*ACLA* Plants

To assess alterations in gene expression from the reduction in ACL activity, cDNA microarray analysis was used to globally profile mRNA accumulation patterns in rosette leaves between wild-type and antisense-*ACLA* plants. These analyses were conducted at the Stanford Arabidopsis Functional Genomic Center (AFGC; expression set, 1005823496 at http://www.arabidopsis.org/servlets/TairObject?type=expression_setandid=1005823496), which enabled the evaluation of the expression patterns of 11,116 unique ESTs representing ~7500 genes. Two hundred and twenty-six of these genes (see Supplemental Table 1 online) show altered expression as assessed by at least a twofold change in the accumulation of the respective mRNA product. Of these, the accumulation of 151 mRNAs increases in antisense-*ACLA* plants, whereas the accumulation of 69 mRNAs decreases in these plants. These genes were functionally categorized (e.g., lipid-related and stress-related) (Figure 12) based on prior literature, AFGC annotations, and additional gene descriptors located via searches of the Aracyc, GenBank, Swiss Prot, and The Arabidopsis Information Resource databases

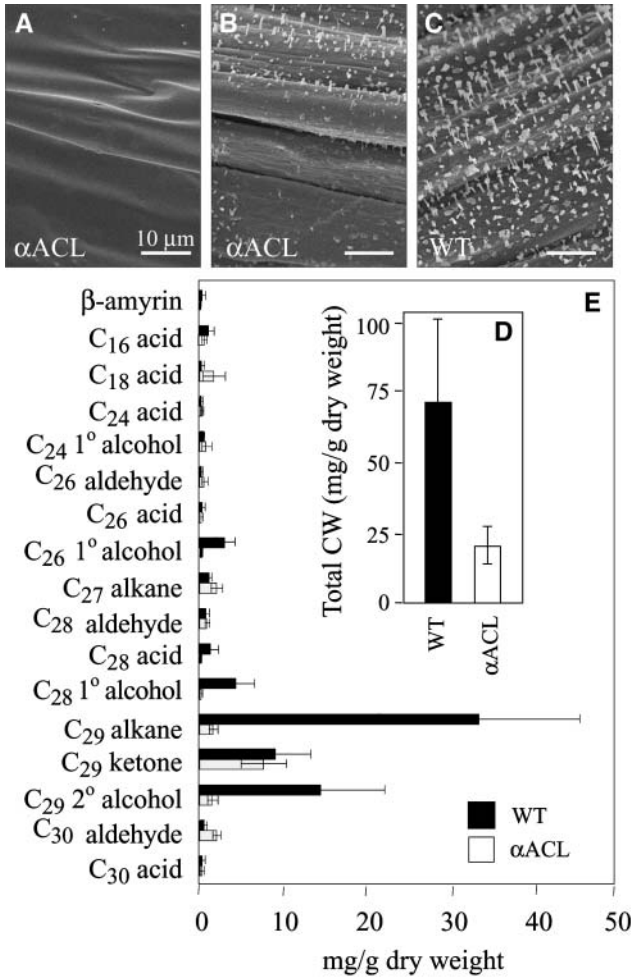

Figure 9. Stems of Antisense-*ACLA* Plants Accumulate Less Wax.

(A) to **(C)** Scanning electron micrographs of basal regions from inflorescence stems of antisense-*ACLA* (αACL) and wild-type plants at 32 DAI showing epicuticular wax crystalloids; five plants of each genotype were examined.

(D) Cuticular wax (CW) load on inflorescence stems of wild-type and αACL plants at 60 DAI.

(E) Major cuticular wax constituents of inflorescence stems of wild-type and αACL plants at 60 DAI. Average data ± SE from three replicate extractions (six plants each).

using AtGeneSearch (http://www.public.iastate.edu/~mash/MetNet/homepage.html).

The eight genes whose expression is most altered (fivefold or greater) in antisense-*ACLA* plants may be indicative of the biological processes that are most sensitive to changes in ACL expression. Three of these genes appear to have diverse functions. These are a putative cytochrome P450 (At3g20940), which is decreased 21-fold; the agamous-like MADS box transcription factor *AGL5* (At2g42830), involved in floral development (Savidge et al., 1995), which is increased 12-fold; and the integrin-related protein 14a (At3g28290), thought to be involved in signal transduction (Nagpal and Quatrano, 1999), which is increased sevenfold.

The other five genes most highly upregulated in the antisense-*ACLA* plants are stress related. These are a lipid-transfer protein, *LTP4* (At5g59310), reportedly induced during cold stress in barley (*Hordeum vulgare*) (Molina et al., 1996), which increases eightfold; an early light induced protein, *ELIP2* (At3g22840), implicated in the protection of the photosynthetic apparatus during desiccation, light, and cold stress (Harari-Steinberg et al., 2001; Hutin et al., 2003), which increases sevenfold; chalcone synthase (At5g13930), a key enzyme in the production of flavonoids (Shirley et al., 1995), often upregulated in response to stress (Schmid et al., 1990), which increases fivefold; and two vegetative storage proteins (At5g24770 and At5g24780) that accumulate in response to jasmonate treatment (Franceschi and Grimes, 1991), which are induced fivefold.

An additional 57 stress-related genes are induced in antisense-*ACLA* plants (Figure 12A). Sixteen of these have been shown to respond to abscisic acid or osmotic stress. Examples are *responsive-to-desiccation 29A* (which is upregulated in response to osmotic stress; Yamaguchi-Shinozaki and Shinozaki, 1993), δ 1-pyrroline-5-carboxylate synthetase (a Pro biosynthetic gene upregulated in association with osmotic stress; Yoshiba et al., 1995), and alcohol dehydrogenase and several putative aldehyde dehydrogenases (upregulation of ALDHs have been associated with dehydration and oxidative stress; Kursteiner et al., 2003; Sunkar et al., 2003).

Another set of stress-related genes that are upregulated in antisense-*ACLA* plants are those involved in the abatement of reactive oxygen species. These include genes coding for glutathione reductase and ascorbate peroxidase (which are enzymes involved in the removal of reactive oxygen; Mittler, 2002) and γ-tocopherol methyltransferase (involved in the production of the antioxidant, α-tocopherol; Mittler, 2002). Other stress-associated genes that are upregulated in antisense-*ACLA* plants encode heat shock proteins (which act as molecular chaperones and protect protein structure during times of cellular stress; Queitsch et al., 2002).

In addition, multiple genes of primary metabolism are downregulated in antisense-*ACLA* plants (Figure 12B). These include two subunits of photosystem II and 12 genes encoding xylosidases and endoxyloglucan transferases, which are required for the formation and rearrangement of cells walls during cell growth (Nishitani and Tominaga, 1992; Goujon et al., 2003). In combination, the upregulation of stress-related genes and the downregulation of genes in primary metabolism and growth suggest that a reduction in cytosolic acetyl-CoA metabolism both places restrictions on normal growth and developmental processes and shifts the plant into a state of stress. These results and conclusions that were obtained with the AFGC microarray experiments are substantiated by ongoing experiments conducted with the Affymetrix-based microarray platform (C.M. Foster and L. Li, personal communication).

DISCUSSION

The inherent chemical properties of the simple, two-carbon molecule acetate, in its activated form, acetyl-CoA, provides organisms with the chemical flexibility to biosynthesize a plethora of natural products that constitute much of the structural and

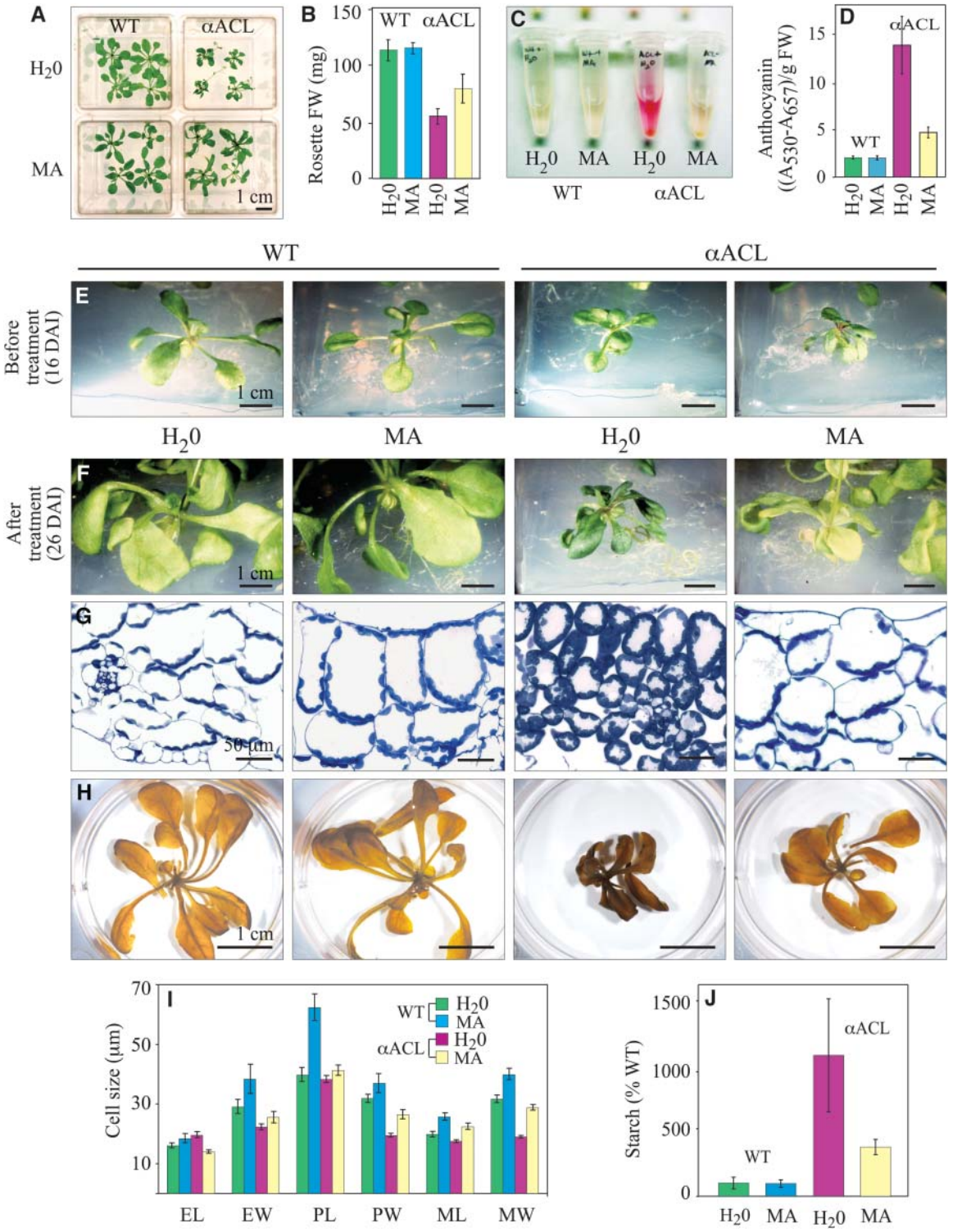

Figure 10. Malonate Chemically Complements the Morphological and Chemical Phenotypes Associated with Reduced ACL Expression.

(A) Wild-type and antisense-*ACLA* (αACL) seedlings at 26 DAI grown either in the presence of water or malonate (MA).

(B) Fresh weight of rosettes of wild-type and αACL seedlings at 26 DAI grown either in the presence of water or malonate. Average ± SE of 16 to 33 determinations.

(C) Methanol-soluble pigment extracts from wild-type and αACL seedlings at 26 DAI grown either in the presence of water or malonate.

functional diversity in nature. This is particularly exemplified in the plant kingdom, where acetyl-CoA metabolism via carboxylation, condensation, or acetylation reactions is used for the production of many different classes of metabolites (Figure 1). By distributing this metabolism among separate cellular and subcellular compartments, plants have the potential of simplifying the regulatory processes that control this complex network. Although the generation of plastidic acetyl-CoA as the precursor for fatty acid biosynthesis has been the focus of considerable research (Millerd and Bonner, 1954; Nelson and Rinne, 1975; Reid et al., 1975; Kuhn et al., 1981; Kaethner and ap Rees, 1985; Burgess and Thomas, 1986; op den Camp and Kuhlemeier, 1997; Ke et al., 2000; Schwender and Ohlrogge, 2002), few studies have directly addressed the question of how the cytosolic (Kaethner and ap Rees, 1985; Fatland et al., 2002; Schwender and Ohlrogge, 2002) or nuclear acetyl-CoA pools are generated. This is despite the fact that most of the chemical diversity of acetate-derived molecules is generated from the cytosolic acetyl-CoA pool.

Our previous characterizations have established that ACL occurs in plants and that its tertiary organization is distinct from the well-characterized animal enzyme (Fatland et al., 2002). Whereas animal ACL is homotetrameric, plant ACL is a heterooctamer, consisting of two subunits, ACLA and ACLB occurring in an A_4B_4 conformation. As in animals, plant ACL is located in the cytosol, thus generating acetyl-CoA in this compartment. To further investigate the physiological role of the ACL-derived cytosolic acetyl-CoA pool, we generated antisense plants with reduced ACL expression.

ACL-Derived Acetyl-CoA Is Nonredundant in Cytosolic Acetyl-CoA Generation

Arabidopsis is highly sensitive to alterations in ACL-derived acetyl-CoA metabolism. Small perturbations in the capacity to generate ACL-derived acetyl-CoA elicit large changes in metabolism, growth, and morphology. Even moderate reductions in ACL activity (e.g., ~50% of wild-type levels) confer this altered phenotype. More extreme reductions in ACL activity (to ~35% of wild-type levels) generate an even more pronounced altered phenotype; such plants do not flower and thus cannot reproduce.

Metabolic redundancy provides organisms with metabolic plasticity, conferring the ability to circumvent stresses and breaches in the metabolic network (Bouche and Bouchez, 2001). This plasticity enables organisms to tolerate mutations and ultimately may be a mechanism that allows pathway evolution (Pichersky and Gang, 2000). As a consequence of such metabolic redundancies, a reduction or elimination of expression of many genes that might be expected to be essential for growth and development leads to no obvious phenotype (Todd et al., 1999; Bouche and Bouchez, 2001).

Our findings demonstrate that ACL is not redundant in generating cytosolic acetyl-CoA; reduced ACL expression creates a severely altered growth phenotype, indicating that the remaining ACL activity is unable to meet the plant's metabolic requirements. Overall, our observations imply that ACL is near-limiting in generating cytosolic acetyl-CoA and that other mechanisms (Wood et al., 1983; Burgess and Thomas, 1986; Masterson et al., 1990) for generating cytosolic acetyl-CoA cannot substitute for ACL-derived acetyl-CoA.

What is the Metabolic Consequence of the Reduction in ACL Expression?

If ACL plays a role in generating cytosolic acetyl-CoA (Figure 1), we hypothesize that a decrease in ACL expression would result in changes in the accumulation of end products of pathways that use this acetyl-CoA pool. Alternately, it is possible that the aberrant phenotype associated with a decrease in ACL may be because of an imbalance of metabolism associated with the other substrates (citrate, ATP, and CoA) or products (ADP, Pi, and oxaloacetate) of the ACL catalyzed reaction.

We have documented that in addition to altering morphology, diminished ACL activity results in specific reductions in the accumulation of cytosolic acetyl-CoA–derived products, namely stem cuticular waxes and seed flavonoids. Moreover, exogenous malonate reverses the reduction of cuticular waxes and alleviates morphological alterations associated with reduced ACL, indicating that the deficiency in cytosolic acetyl-CoA (rather than the other ACL reactants and products) is responsible for the antisense-*ACLA* phenotype. Presumably, the applied malonate is converted to malonyl-CoA in the cytosol by an as yet unidentified malonyl-CoA synthetase. One of several Arabidopsis genes with sequences similar to short chain acyl-CoA synthetase enzymes (Shockey et al., 2003) may provide this biochemical function. Our data therefore indicate that a decrease in acetyl-CoA generation per se and its subsequent flow into the carboxylation pathway is probably responsible for the antisense-*ACLA* phenotype. The importance of the acetyl-CoA carboxylation

Figure 10. (continued).

(D) Anthocyanin concentration in methanol extracts from wild-type and αACL seedlings at 26 DAI grown either in the presence of water or malonate. Average ± SE of three determinations of two to three pooled plants.

(E) and **(F)** Wild-type and αACL seedlings (at 16 DAI) **(E)**; the same seedlings (at 26 DAI) 10 d after treatment with water or malonate **(F)**.

(G) Micrographs of leaf cross sections from wild-type and αACL plants grown either in the presence of water or malonate.

(H) IKI-stained wild-type and αACL seedlings grown either in the presence of water or malonate.

(I) Dimensions (length, L; width, W) of epidermal (E), palisade (P), and mesophyll (M) cells of αACL and wild-type leaves of plants at 26 DAI. For each genotype, the average dimension ± SE was determined from 6 to 57 cells of midleaf cross sections taken from each of four separate plants.

(J) Starch content in wild-type and αACL seedlings grown either in the presence of water or malonate. Average ± SE of three determinations (two to four plants pooled for each determination).

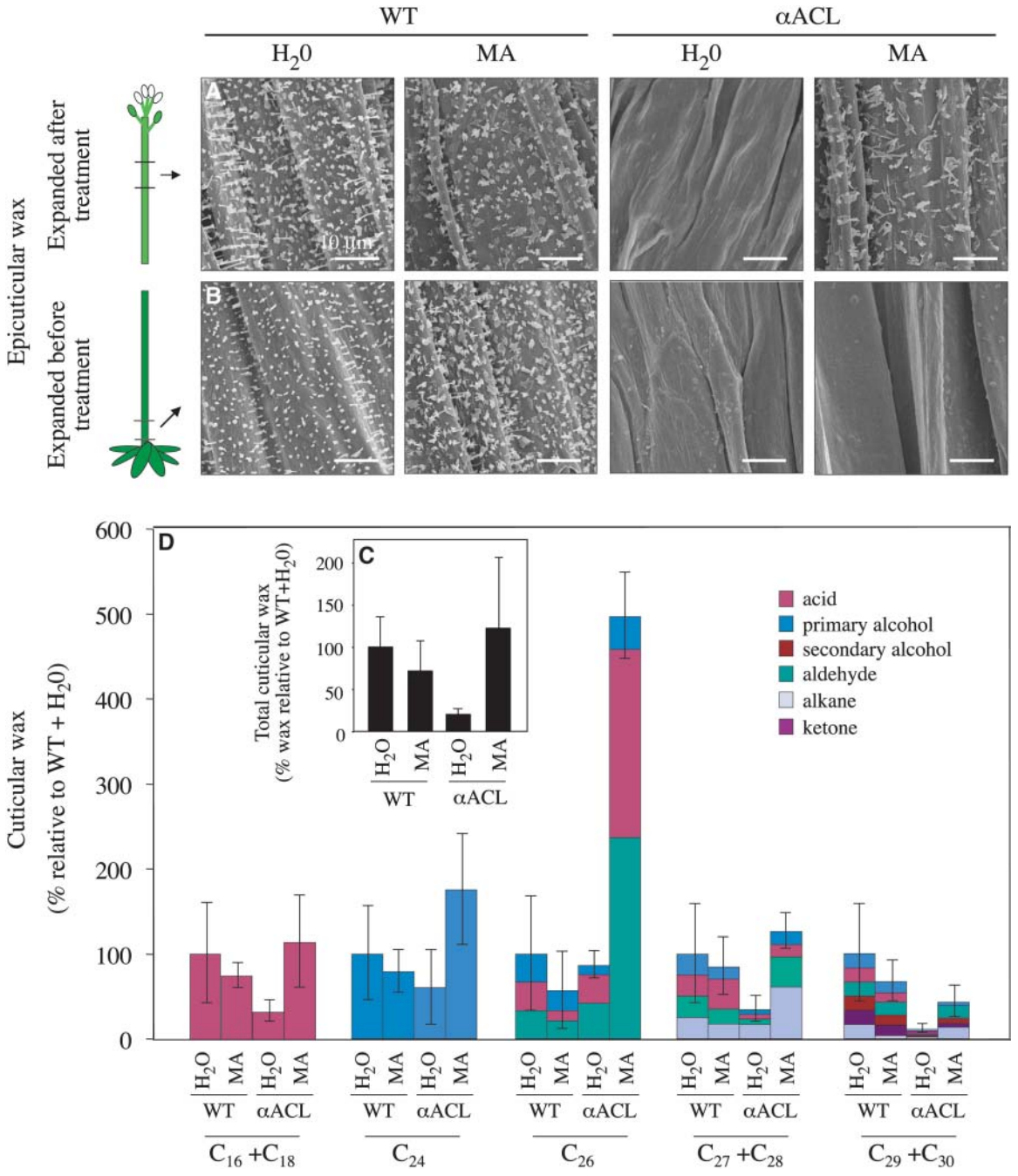

Figure 11. Malonate Treatment Leads to the Recovery of Cuticular Wax Accumulation on Antisense-*ACLA* Plants.

Scanning electron micrographs of epicuticular wax on inflorescence stems of wild-type and antisense-*ACLA* (αACL) plants before **(B)** and after **(A)** treatment with water or malonate (MA).

(A) Stem segments that expanded after treatment.

(B) Stem segments that expanded before treatment.

(C) Chloroform-soluble cuticular wax load on inflorescence stems of wild-type and αACL plants treated with water or malonate, normalized relative to water-treated wild-type plants.

(D) Concentration of cuticular wax constituents categorized by their carbon chain lengths and chemical class. Bars represent ±SE associated with three extractions of six pooled stems.

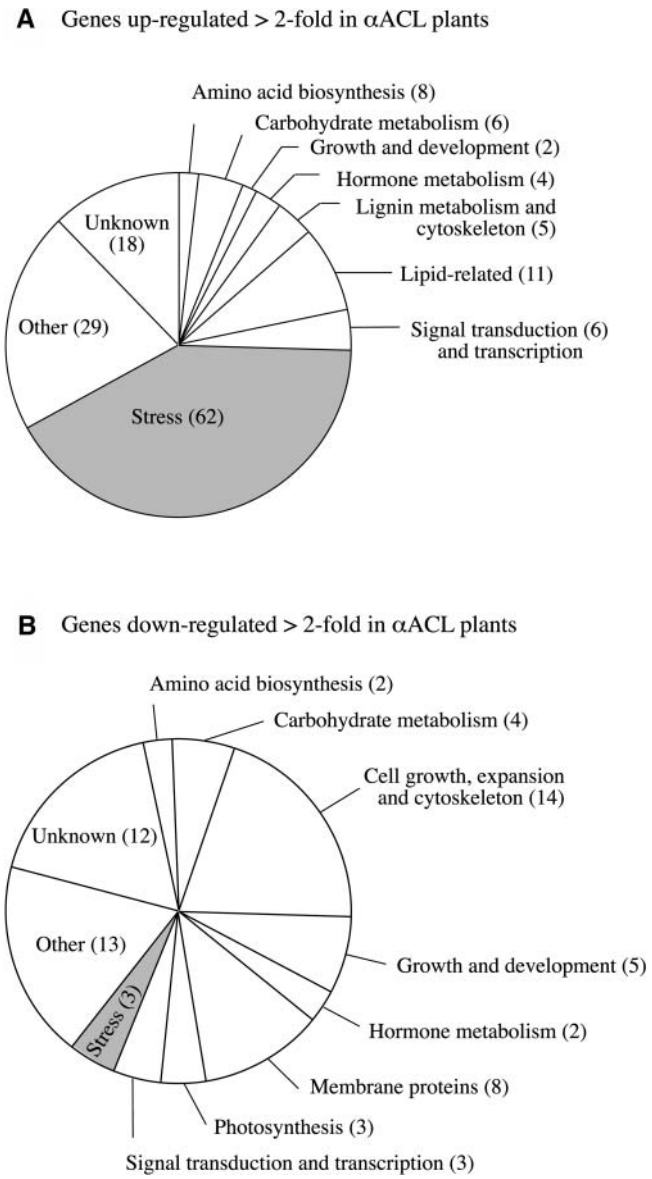

Figure 12. cDNA Microarray Analysis Reveals Specific Trends in mRNA Accumulation in Antisense-*ACLA* Plants.

Functional categorization of mRNAs that differentially accumulate between antisense-*ACLA* (αACL) and wild-type rosettes; the number of mRNAs within each category is in parentheses.
(A) mRNAs that increase in αACL plants.
(B) mRNAs that decrease in αACL plants. See Supplemental Table 1 online for identity of these genes.

pathway is not only revealed by our findings, but is also illustrated by the embryo-lethal phenotype that is associated with mutations in the *acc1* gene that codes for the cytosolic acetyl-CoA carboxylase and commits carbon to the acetyl-CoA carboxylation pathway (Baud et al., 2002, 2004). Indeed, these *acc1* mutants are also able to be rescued by exogenous malonate. These observations are consistent with the essential nature of the pathways derived from acetyl-CoA carboxylation (i.e., malonyl-CoA).

Unexpectedly, antisense-*ACLA* plants hyperaccumulate anthocyanins and starch in vegetative tissue. Given the centrality and complexity of ACL-associated metabolism, these pleiotropic effects are not necessarily surprising but may reveal novel metabolic regulatory connections. Prior studies have shown that anthocyanins and/or starch hyperaccumulate during many different stresses (von Schaewen et al., 1990; Riesmeier et al., 1994; Nemeth et al., 1998; Shirley, 2002), which may indicate that these antisense-*ACLA* plants are perceiving a physiological stress that we term ''metabolic stress.'' The perception of this stress may prioritize the commitment of the limited acetyl-CoA pool to anthocyanin biosynthesis.

It is unclear how a block in cytosolic acetyl-CoA metabolism redirects the commitment of carbon into starch deposition. However, the fact that malonate supplementation alleviates both of these effects indicates it is related to the carboxylation pathway of cytosolic acetyl-CoA metabolism.

The simplest explanation of the ability of malonate to supplement the antisense-*ACLA* phenotype is that a decrease of a single acetyl-CoA–derived metabolite in the carboxylation pathway is responsible for the antisense-*ACLA* phenotype. Because independent discreet mutants in such metabolic pathways (e.g., flavonoid biosynthesis, Shirley et al., 1995; and cuticular wax biosynthesis; Koorneef et al., 1989; Jenks et al., 1996; Todd et al., 1999) do not show this complex phenotype, it would suggest that the antisense-*ACLA* phenotype is not because of a deficiency of flavonoid or cuticular wax constituents, but rather deficiencies in other metabolites, such as sphingolipids, or multiple malonate-derived compounds. Alternatively, exogenous malonate may be alleviating the demand for acetyl-CoA by the carboxylation pathway, thereby allowing acetyl-CoA to be used for the other competing pathways (i.e., the condensation and acetylation pathways).

ACL-Centered Regulatory Loops

Plant ACL is a heterooctamer consisting of ACLA and ACLB subunits. In Arabidopsis, each subunit is encoded by a small gene family; three genes code for the ACLA subunit and two genes code for the ACLB subunit. In situ hybridization data established the coordinate accumulation of ACLA and ACLB mRNAs to meet tissue requirements at discreet developmental times (Fatland et al., 2002).

Our characterization of plants with reduced ACL reveals the occurrence of both proximal and distal ACL-centered regulatory loops. One example of a proximal regulatory loop encompasses the ACLA and ACLB subunits. That a reduction in the ACLA subunit concomitantly reduces the accumulation of the ACLB subunit implies that a mechanism must exist that coordinates the accumulation of these two subunits. This is unusual; to our knowledge, only for ribulose-1,5-bisphosphate carboxylase/oxygenase has a similar example of coreduction in both subunits been reported (Rodermel et al., 1996). Although the protein coding exons of *ACLA-2* and *ACLA-3* share 89 and 78% identity in nucleotide sequence, and *ACLB-1* and *ACLB-2* share 88% sequence identity, there is no sequence similarity between any of the *ACLA* and *ACLB* genes. Therefore, this coordination in expression is not a cosuppression mechanism. Rather, this

mechanism may affect the transcription or translation of the ACLB genes or mRNAs, respectively, or it may be posttranslational processing (e.g., excess ACLB subunit may be turned over in the absence of ACLA). As would be expected from the sequence similarity, Affymetrix-based microarray experiments (C.M. Foster and L. Li, personal communication) indicate that accumulation of all three *ACLA* mRNAs (*ACLA-1*, *ACLA-2*, and *ACLA*-3) are reduced by ~30% in antisense-*ACLA* plants. However, the accumulation of the *ACLB-1* and *ACLB-2* mRNAs is unaffected. We therefore speculate that coordination between *ACLA* and *ACLB* expression is via a posttranscriptional mechanism.

Our microarray analyses begin to reveal the scope of the distal ACL-centered regulatory loops. In several instances, alterations in the accumulation of specific mRNAs can be interpreted in terms of phenotypic alterations in the antisense-*ACLA* plants. For example, the reduced expression of multiple xylosidases and endoxyloglucan transferases, which are involved in cell wall expansion and secondary cell wall thickening (Nishitani and Tominaga, 1992; Goujon et al., 2003), parallels the reduction in cell size. The upregulation of chalcone synthase correlates with the hyperaccumulation of anthocyanin in vegetative tissues. In conjunction, the increased accumulation of many stress-related mRNAs provides mechanistic insights into the visibly perturbed state of the antisense-*ACLA* plants; clearly, these plants are under physiological stress. The expression of stress-related genes is elevated, consistent with the concept of metabolic stress.

The ability of malonate to rescue many, if not all, of the observed phenotypes associated with reduced ACL expression indicates that the metabolic deficiency that gives rise to this altered phenotype is associated with the carboxylation branch of cytosolic acetyl-CoA metabolism.

METHODS

Recombinant DNA Construction

The near full-length *ACLA-1* cDNA (1.53 kb) (GenBank accession number Z18045; Fatland et al., 2002) was cloned in the antisense orientation into a modified (Qian, 2002) pBI121L plasmid (BD Biosciences Clontech, Palo Alto, CA) (Sambrook et al., 1989). This cloning placed the antisense-*ACLA-1* cDNA under control of the CaMV 35S constitutive promoter. The resultant plasmid (p35S:antisense-*ACLA-1*) was introduced into *Agrobacterium tumefaciens* (strain C58C1) by electroporation (Sambrook et al., 1989).

Plant Transformation and Selection

Arabidopsis thaliana Columbia ecotype (Lehle Seeds, Round Rock, TX) was transformed using an Agrobacterium-mediated protocol adapted from Bechtold et al. (1993) and Bent et al. (1994). Inflorescence bolts of 40-DAI plants were submerged for 5 min in infiltration medium containing *A. tumefaciens* (strain C58C1) possessing p35S:antisense-*ACLA-1*. Infiltration medium consisted of 0.22% MS (Murashige, 1973) salt mixture (Invitrogen, Carlsbad, CA), 1× B5 vitamins, 5% sucrose, 0.05% Mes-KOH, pH 7.0, 44 nM benzylaminopurine, and 0.02% Silwet L-77 (OSI Specialties, South Charleston, WV). Plants were returned to a 22°C growth chamber under continuous illumination (210 μmol m^{-2} s^{-1}) until seed harvest.

In preparation for selecting transformation events, seeds were germinated in the presence of lethal doses of kanamycin (30 μg/mL) (Bent et al., 1994). Eight to 10 DAI, kanamycin-resistant seedlings were transferred to soil and propagated.

PCR Analysis

The PCR protocol outlined by Klimyuk et al. (1993) was used to confirm the presence of the 35S:antisense-*ACLA-1* transgene in the genome. Primers were designed to amplify a 1.4-kb sequence of the 35S:antisense-*ACLA-1* construct. Forward primer sequence, p-F (5′-ACTATCCTTCGCAAGACCCTT-3′), was designed to anneal to sequence near the end of the CaMV 35S promoter. The reverse primer sequence, p-R (5′-AGGAACCTTGGCTCTCGTCT-3′), was designed to anneal to the 3′ end of the *ACLA-1* sequence. The resulting PCR products were analyzed by agarose gel electrophoresis.

Plant Growth Conditions

For characterization of the antisense-*ACLA* phenotype, PCR-confirmed T2 and T3 seeds were grown on either 60 mL of MS agar solid media in magenta boxes (in the absence of kanamycin) under continuous illumination (170 μmol m^{-2} s^{-1}) at 22°C or in sterile LC1 Sunshine Mix soil (Sun Gro Horticulture, Bellevue, WA) under continuous illumination (210 μmol m^{-2} s^{-1}) at 22°C. To avoid insect infestation, the soil was treated with ~1 g of 1% granular Marathon (Olympic Horticultural Products, Bradenton, FL). Plant were watered once a week and supplemented every other week with a 20-nitrogen:10-phosphorous:20-potassium fertilizer mix (Plant Marvel Laboratory, Chicago Heights, IL).

Measurement of Plant Growth

Root length was determined from seedlings grown on MS agar solid media in vertically placed Petri dishes. The diameter of the rosettes was measured at the widest point, and the height of the bolt above the youngest rosette leaf was determined.

Protein Gel Blot Analyses

Protein extracts were subjected to SDS-PAGE (Laemmli, 1970) and protein gel blotting with ACL antibodies (Fatland et al., 2002) or ^{125}I-streptavidin (Nikolau et al., 1985). Radioactive bands were detected using a STORM 840 PhosphorImager (Molecular Dynamics, Sunnyvale, CA). The resulting band intensities were quantified using ImageQuant software, version 1.2 (Molecular Dynamics). The immunologically detected ACLA and ACLB band intensities were normalized relative to the biotin containing subunit of 3-methylcrotonyl-CoA carboxylase (Che et al., 2002), which was detected with streptavidin. This quantification was conducted on 20 wild-type plants and 10 to 18 antisense-*ACLA* plants from each phenotype category.

ACL Activity Assay

Protein extracts were desalted by chromatography through Sephadex G-25 (Sigma-Aldrich, St. Louis, MO), and ACL activity was determined using a coupled spectrophotometric assay (Takeda, 1969; Fatland et al., 2002).

Light and Transmission Electron Microscopy

Leaf discs were fixed in a solution consisting of 1% paraformaldehyde and 2% glutaraldehyde in 65 mM cacodylate buffer at pH 7.2. After a 21-h fixation at 4°C, leaf pieces were washed three times in 65 mM cacodylate buffer, pH 7.2, immersed in 1% osmium tetroxide in 65 mM cacodylate buffer, and fixed for an additional hour. Osmicated samples were rinsed once with buffer and twice with deionized water and then dehydrated

through a series of graded concentrations of ethanol (50, 70, 85, 95, and 100%). To embed the leaf discs, they were serially infiltrated with ethanol:acetone (1:1), acetone, acetone:Spurr's resin (1:1), and finally 100% Spurr's resin (EM Sciences, Fort Washington, PA) and polymerized by incubation at 60°C for 48 h.

One micrometer–thick leaf discs were sectioned with a Reichert Ultracut S Ultramicrotome (North Central Instruments, Minneapolis, MN), stained with 1% toluidine blue, and observed under bright-field optics on a Leitz orthoplan microscope (Sciscope; Leica, Iowa City, IA) or a Zeiss Axioplan 2 compound light microscope (Carl Zeiss, Thornwood, NY). To examine fresh inflorescence stems, 60-μm thick sections were cut with a Vibratome Series 3000 (Technical Products International, St. Louis, MO). The sections were placed in a drop of water on a glass slide, covered with a cover slip, and examined as described. For stereomicrography, an Olympus SZH10 camera (Tokyo, Japan) or an AxioCam HRC digital camera mounted on an Olympus SZH10 35-mm research stereomicroscope was used for image collection.

For transmission electron microscopy, 60 nm–thick sections were stained with 5% uranyl acetate in methanol and Sato's lead stain (Sato, 1967) and observed with a JEOL 1200 EX scanning transmission electron microscope (Japan Electron Optics Laboratory, Peabody, MA).

Scanning Electron Microscopy

Fresh basal inflorescence stem segments were harvested and prepared for scanning electron microscopy analysis using a protocol based on that of Jenks et al. (1995). After samples were sputter-coated with a 20/80 gold-palladium alloy for four, 30-s bursts, they were examined at 10 kV on a JEOL 5800 LV scanning electron microscope (Japan Electron Optics Laboratory).

Polysaccharide Cytochemistry

Leaf sections of 1-μm and 60-nm thickness were processed through the Thiery reaction (Hall, 1978). Sections on glass slides or grids were treated for 45 min with 1% periodic acid (which oxidizes vicinal diols to aldehydes) or with 10% hydrogen peroxide (as a control to monitor nonspecific oxidative production of aldehydes). After four, 5-min washes with deionized water, all sections were treated for 18 h with 0.2% thiocarbohydrazide at room temperature. Sections were then washed twice for 5 min each in 20, 10, and 5% acetic acid and three times in deionized water. Washed sections were treated with silver proteinate in the dark for 130 min and subsequently processed through four, 5-min distilled water washes. The electron-dense complexes, formed by reaction of silver proteinate with thiocarbohydrazide, were visualized by light microscopy.

Starch Staining

Starch was stained with IKI (Berlyn et al., 1976). Seedlings were incubated for 48 h in 95% ethanol to remove pigments and then incubated overnight in a solution containing 1% IKI and 1% iodine. Seedlings were rinsed with water for ~30 min and photographed.

Starch Quantification

Starch from rosettes was extracted using a modified protocol based on that of Zeeman et al. (1998). Approximately 0.3 g of rosettes were boiled in 80% ethanol for at least 30 min, until tissue was decolorized. The tissue was then homogenized in a fresh aliquot of 80% ethanol, and the resulting slurry was centrifuged for 10 min at 1500*g*. The resulting pellet was washed with 80% ethanol and resuspended in 1 or 2 mL of water (the wild type and antisense-*ACLA*, respectively). The extract was boiled for 30 min. Total glucan content was quantified using a starch quantification kit (R-Biopharm, Marshall, MI), which measures glucose released after digestion with amyloglucosidase.

Pigment Quantification

A single spectrophotometric protocol (Lichtenthaler, 1987) was used to determine the concentration of photosynthetic pigments. Rosettes, ranging from 50 to 300 mg FW, were pulverized in liquid nitrogen and extracted by vortexing for 30 s with 4 mL of 95% ethanol and incubated at 4°C in the dark for 5 h. After centrifugation for 10 min at 1500*g*, the supernatant was retained, and pellet was further extracted with a fresh aliquot of 95% ethanol. Ethanol extracts were combined and their absorbance at 664, 649, and 470 nm was determined, respectively, measuring chlorophyll *a*, chlorophyll *b*, and carotenoids.

Anthocyanin content was assessed using a protocol based on that of Rabino and Mancinelli (1986) and Bariola et al. (1999). Rosettes (75 to 300 mg FW) were frozen in liquid nitrogen and pulverized. The resultant powder was extracted by shaking at room temperature for 2 h with 10 volumes of 1% HCl in methanol. To remove interfering pigments, 8 volumes of chloroform was added, and the samples were vortexed for 1 min. Deionized water (20 volumes) was added, and the samples were vortexed for 1 min and centrifuged (5 min at 1500*g*). The absorbance of the upper, methanol/water, phase was determined at 530 and 657 nm. Anthocyanin concentration was calculated from the difference in absorbance (A_{530} to A_{657}).

Anthocyanin concentrations were determined from seeds as for leaves, with the exception that 10 to 27 mg of seed was used per extraction and the seeds were extracted with 2N HCl (Albert et al., 1997).

Extraction and Analysis of Fatty Acids from Seed

Lipids were extracted from batches of 100 seeds using a protocol based on that of James and Dooner (1991). Internal standard (17 μg of triheptadecanoate [Fluka, Buchs, Switzerland] in hexane) was applied to the sample, and seeds were homogenized in 1N HCl in methanol for 2 min. An aliquot of this slurry was transmethylated by incubating an aliquot of this slurry under a nitrogen atmosphere at 80°C for 1 h. The reaction was stopped by the addition of 1 mL of 0.9% NaCl, and fatty acid methyl esters were extracted with three aliquots of hexane. Hexane extracts were pooled, filtered through a 0.22-μm polytetrafluoroethylene filter (Alltech, Deerfield, IL), and concentrated by evaporation under a stream of nitrogen gas. Fatty acid methyl esters were analyzed using a GC series 6890 from Agilent (Palo Alto, CA) equipped with an HP-1 silica capillary column (30 m × 0.32 μm, inner diameter), using helium as the carrier gas. The GC series 6890 was coupled to a 5973 Agilent mass detector. The injector was held at 250°C. The oven was at 80°C for 5 min, then ramped at 5°C/min to 260°C and maintained at this temperature for 10 min, and then ramped at 5°C/min to 320°C and maintained at this temperature for 30 min. Resulting chromatograms were integrated by Agilent's HP enhanced ChemStation TM G1701 BA version B.01.00 software. Peaks were identified by comparing acquired mass spectra with GLOSSY (Perera et al., 2003) and Agilent NIST98 mass spectra libraries. Quantity of fatty acid/mg FW seed was calculated based on the internal standard.

Wax Extraction and Analysis

Cuticular waxes were extracted using a modified protocol of Perera et al. (2003), optimized for Arabidopsis. Primary bolts from antisense-*ACLA* plants showing a severe phenotype were harvested at the base of the stem, cauline leaves were removed, and bolts were weighed. A known amount of hexadecane (Sigma-Aldrich) was applied, as an internal standard, to the surface of the stem before extraction. Chloroform-soluble waxes were extracted by dipping 0.2 to 0.3 g FW of plant material

into 60 mL of chloroform for 60 s. The chloroform extract was filtered through glass wool into a round bottom flask and concentrated by evaporation at 30°C using a rotary vacuum evaporator. Chloroform-dissolved wax samples were silylated using a protocol based on that of Wood et al. (2001) and Hannoufa et al. (1993). Specifically, nitrogen-dried wax extract was dissolved in 1 mL of acetonitrile and adjusted to 6% of bis-trimethylsilyl-trifluoroacetamide and 10% trimethyl-chlorosilane. Samples were incubated at 100°C for 30 min, cooled, suspended in chloroform, and filtered through a polytetrafluoroethylene filter. Silylated cuticular wax samples were analyzed using a GC series 6890 from Agilent equipped with an HP-1 silica capillary column (30 m × 0.32 μm, inner diameter) using helium as the carrier gas. The GC series 6890 was coupled to a 5973 Agilent mass detector. The injector was held at 250°C. The oven was initially at 80°C for 5 min, then ramped at 5°C/min to 260°C and held for 10 min, and then ramped at 5°C/min to 320°C and held for 30 min. Resulting chromatograms were integrated by Agilent's HP enhanced ChemStation TM G1701 BA version B.01.00 software. Peaks were identified by comparing acquired mass spectra with the GLOSSY (Perera et al., 2003) and Agilent NIST98 mass spectra libraries. The quantity of wax/g dry weight of plant material was calculated based on the internal standard.

Biochemical Complementation

To monitor the extent to which external biochemicals revert the antisense-*ACLA*–associated phenotype, wild-type and antisense-*ACLA* plants were grown on 60 mL of MS agar media in magenta boxes (four seedlings per box). At 15 to 18 DAI, the phenotype associated with each seedling was determined, and either 0.25 mL of filter-sterilized water or 0.25 mL of an alternate biochemical solution was directly applied by pipetting to the base of each plant. Biochemicals that were tested include the following: acetate (0.6 mM), malonate (0.6 mM), narigenin (0.36 and 4.2 mM), *O*-acetyl-Ser (0.6 mM), oxaloacetate (120 mM), phosphoenolpyruvate (120 mM), stilbene (3 mM), and amino acid mixtures (Sigma-Aldrich), including proteinaceous amino acids plus β-Ala, L-α-aminoadipic acid, L-α-amino-*n*-butyric acid, γ-amino-*n*-butyric acid, DL-β-aminoisobutyric acid, L-anserine, L-carnosine, L-citrulline, creatinine, cystathionine, ethanolamine, L-homocystine, δ-Hyl, hydroxy-L-Pro, 1-methyl-L-histidine, 3-methyl-L-histidine, L-Orn, *O*-phospho-L-Ser, *O*-phosphoethanolamine, sarcosine, and taurine (15 mM). Ten days after this treatment (25 to 28 DAI), seedlings were weighed, and the accumulation of cuticular waxes, starch, and anthocyanins was determined. In addition, tissue was harvested for microscopic examination.

Microarray Analysis

The rosettes of soil-grown wild-type plants and antisense-*ACLA* plants demonstrating a severe phenotype were harvested at 33 DAI. RNA was extracted from ~1.5 g of wild-type rosettes (equivalent to four seedlings) and antisense-*ACLA* rosettes (equivalent to 30 seedlings) using a TRIzol-based extraction protocol (AFGC). Poly(A)$^+$ RNA was purified using the Qiagen Oligotex mRNA mini kit (Valencia, CA). Poly(A)$^+$ RNA was sent to the AFGC Microarray Facility (Stanford, CA) for cDNA microarray analysis.

Cy3- and Cy5-labeled cDNAs created by reverse transcription of Poly(A)$^+$ RNA were hybridized on microarray chips containing cDNA spots representing 11,116 unique EST clones (Newman et al., 1994). Both Cy3- and Cy5-dye combinations of the two samples (wild-type and antisense-*ACLA* plants) were hybridized to two separate microarrays.

Analysis of variance (ANOVA) was conducted on 9376 of 11,483 log ratios of normalized mean intensities. Empty spots, spots flagged as bad by AFGC, spots with saturated intensities, and spots with raw mean intensities less than two times median background were removed from the analysis. ANOVA and determination of significance were conducted as outlined by Qian (2002).

Sequence data from this article have been deposited with the EMBL/GenBank data libraries under accession number Z18045.

ACKNOWLEDGMENTS

We are grateful to Ann Perera for helpful discussion on cuticular wax analysis and for guidance during the use of equipment at the W.M. Keck Metabolomics Facility and to Harry Horner and Tracey Pepper for helpful discussion and for use of equipment at the Iowa State University Bessey Microscopy Facility. We thank Hilal Ilarslan for helpful discussions and for the inflorescence stem micrographs (Figures 3W to 3Z), fixing and sectioning MA-treated plants (Figure 10G), and additional sectioning on antisense-*ACLA* leaves. We thank Hui-Rong Qian for the ANOVA and additional analysis of the microarray data. We gratefully acknowledge Carol Foster, Marty Spalding, and Ron Mittler for helpful discussions. We are grateful to the W.M. Keck Metabolomics Facility for the use of their equipment. We are grateful to the Department of Energy (Grant DE-FG02-01ER15170), the USDA (2000-03447), the National Science Foundation 2010 (DBI-0209809), and the Consortium for Plant Biotechnology Research (OR22072-73 and GO12026-158) for funding this project.

Received July 20, 2004; accepted October 9, 2004.

REFERENCES

Albert, S., Delseny, M., and Devic, M. (1997). BANYULS, a novel negative regulator of flavonoid biosynthesis in the Arabidopsis seed coat. Plant J. **11,** 289–299.

Bao, X., Pollard, M., and Ohlrogge, J. (1998). The biosynthesis of erucic acid in developing embryos of *Brassica rapa*. Plant Physiol. **118,** 183–190.

Bariola, P.A., MacIntosh, G.C., and Green, P.J. (1999). Regulation of S-like ribonuclease levels in Arabidopsis. Antisense inhibition of RNS1 or RNS2 elevates anthocyanin accumulation. Plant Physiol. **119,** 331–342.

Baud, S., Bellec, Y., Miquel, M., Bellini, C., Caboche, M., Lepiniec, L., Faure, J.D., and Rochat, C. (2004). gurke and pasticcino3 mutants affected in embryo development are impaired in acetyl-CoA carboxylase. EMBO Rep. **5,** 515–520.

Baud, S., Guyon, V., Kronenberger, J., Wuillème, S., Miquel, M., Caboche, M., Lepiniec, L., and Rochat, C. (2002). Multifunctional acetyl-CoA carboxylase 1 is essential for very long chain fatty acid elongation and embryo development in Arabidopsis. Plant J. **33,** 75–86.

Bechtold, N., Ellis, J., and Pelletier, G. (1993). In planta *Agrobacterium*-mediated transformation of adult *Arabidopsis thaliana*. Methods Mol. Biol. **82,** 259–266.

Behal, R.H., Lin, M., Back, S., and Oliver, D.J. (2002). Role of acetyl-coenzyme A synthetase in leaves of *Arabidopsis thaliana*. Arch. Biochem. Biophys. **402,** 259–267.

Bent, A.F., Kunkel, B.N., Dahlbeck, D., Brown, K.L., Schmidt, R., Giraudat, J., Leung, J., and Staskawicz, B.J. (1994). RPS2 of *Arabidopsis thaliana*: A leucine-rich repeat class of plant disease resistance genes. Science **265,** 1856–1860.

Berlyn, G.P., Miksche, J.P., and Sass, J.E. (1976). Botanical Microtechnique and Cytochemistry. (Ames, IA: Iowa State University Press).

Bloor, S.J., and Abrahams, S. (2002). The structure of the major anthocyanin in *Arabidopsis thaliana*. Phytochemistry **59,** 343–346.

Bohn, M., Heinz, E., and Luthje, S. (2001). Lipid composition and fluidity of plasma membranes isolated from corn (*Zea mays* L.) roots. Arch. Biochem. Biophys. **387,** 35–40.

Bouche, N., and Bouchez, D. (2001). Arabidopsis gene knockout: Phenotypes wanted. Curr. Opin. Plant Biol. **4,** 111–117.

Brooks, J.L., and Stumpf, P.K. (1966). Fat metabolism in higher plants. XXXIX. Properties of a soluble fatty acid synthesizing system from lettuce chloroplasts. Arch. Biochem. Biophys. **116,** 108–116.

Burgess, B., and Thomas, D.R. (1986). Carnitine acetyltransferase in pea cotyledon mitochondria. Planta **167,** 58–65.

Che, P., Wurtele, E.S., and Nikolau, B.J. (2002). Metabolic and environmental regulation of 3-methylcrotonyl-coenzyme A carboxylase expression in Arabidopsis. Plant Physiol. **129,** 625–637.

Choi, C.H., Hiromura, M., and Usheva, A. (2003). Transcription factor IIB acetylates itself to regulate transcription. Nature **424,** 965–969.

Clouse, S.D. (2002). Arabidopsis mutants reveal multiple roles for sterols in plant development. Plant Cell **14,** 1995–2000.

Desfeux, C., Clough, S.J., and Bent, A.F. (2000). Female reproductive tissues are the primary target of Agrobacterium-mediated transformation by the Arabidopsis floral-dip method. Plant Physiol. **123,** 895–904.

Disch, A., Schwender, J., Muller, C., Lichtenthaler, H.K., and Rohmer, M. (1998). Distribution of the mevalonate and glyceraldehyde phosphate/pyruvate pathways for isoprenoid biosynthesis in unicellular algae and the cyanobacterium Synechocystis PCC 6714. Biochem. J. **333,** 381–388.

Eccleston, V.S., and Ohlrogge, J.B. (1998). Expression of lauroyl-acyl carrier protein thioesterase in *Brassica napus* seeds induces pathways for both fatty acid oxidation and biosynthesis and implies a set point for triacylglycerol accumulation. Plant Cell **10,** 613–622.

Falk, K.L., Vogel, C., Textor, S., Bartram, S., Hick, A., Pickett, J.A., and Gershenzon, J. (2004). Glucosinolate biosynthesis: Demonstration and characterization of the condensing enzyme of the chain elongation cycle in *Eruca sativa*. Phytochemistry **65,** 1073–1084.

Fatland, B.L., Ke, J., Anderson, M.D., Mentzen, W.I., Cui, L.W., Allred, C.C., Johnston, J.L., Nikolau, B.J., and Wurtele, E.S. (2002). Molecular characterization of a heteromeric ATP-citrate lyase that generates cytosolic acetyl-coenzyme A in Arabidopsis. Plant Physiol. **130,** 740–756.

Franceschi, V.R., and Grimes, H.D. (1991). Induction of soybean vegetative storage proteins and anthocyanins by low-level atmospheric methyl jasmonate. Proc. Natl. Acad. Sci. USA **88,** 6745–6749.

Givan, C.V. (1983). The source of acetyl coenzyme A in chloroplasts of higher plants. Physiol. Plant. **57,** 311–316.

Goujon, T., Minic, Z., El Amrani, A., Lerouxel, O., Aletti, E., Lapierre, C., Joseleau, J.P., and Jouanin, L. (2003). AtBXL1, a novel higher plant (*Arabidopsis thaliana*) putative beta-xylosidase gene, is involved in secondary cell wall metabolism and plant development. Plant J. **33,** 677–690.

Hall, J.L. (1978). Electron Microscopy and Cytochemistry of Plant Cells. (New York: Elsevier/North-Holland Biomedical Press).

Hannoufa, A., McNevin, J., and Lemieux, B. (1993). Epicuticular waxes of *eceriferum* mutants of *Arabidopsis thaliana*. Phytochemistry **33**, 851–855.

Harari-Steinberg, O., Ohad, I., and Chamovitz, D.A. (2001). Dissection of the light signal transduction pathways regulating the two early light-induced protein genes in Arabidopsis. Plant Physiol. **127,** 986–997.

Hayat, M.A. (2000). Osmium tetroxide. In Principles and Techniques of Electron Microscopy: Biological Applications, M.A. Hayat, ed (New York: Cambridge University Press), pp. 45–46.

Hohl, H.U., and Barz, W. (1995). Metabolism of the insecticide phoxim in plants and cell suspension cultures of soybean. J. Agric. Food Chem. **43,** 1052–1056.

Hrazdina, G., Wager, G.J., and Siegelman, H.W. (1978). Subcellular localization of enzymes of anthocyanin biosynthesis in plants. Phytochemistry **17,** 53–56.

Hutin, C., Nussaume, L., Moise, N., Moya, I., Kloppstech, K., and Havaux, M. (2003). Early light-induced proteins protect Arabidopsis from photooxidative stress. Proc. Natl. Acad. Sci. USA **100,** 4921–4926.

James, D.W., and Dooner, H.K. (1991). Novel seed lipid phenotypes in combinations of mutants altered in fatty acid biosynthesis in Arabidopsis. Theor. Appl. Genet. **82,** 409–412.

Jenks, M.A., Rashotte, A.M., Tuttle, H.A., and Feldmann, K.A. (1996). Mutants in *Arabidopsis thaliana* altered in epicuticular wax and leaf morphology. Plant Physiol. **110,** 377–385.

Jenks, M.A., Tuttle, H.A., Eigenbrode, S.D., and Feldmann, K.A. (1995). Leaf epicuticular waxes of the *eceriferum* mutants in Arabidopsis. Plant Physiol. **108,** 369–377.

Kaethner, T.M., and ap Rees, T. (1985). Intracellular location of ATP citrate lyase in leaves of *Pisum sativum* L. Planta **163,** 290–294.

Ke, J., Behal, R.H., Back, S.L., Nikolau, B.J., Wurtele, E.S., and Oliver, D.J. (2000). The role of pyruvate dehydrogenase and acetyl-coenzyme A synthetase in fatty acid synthesis in developing Arabidopsis seeds. Plant Physiol. **123,** 497–508.

Keppler, D., and Decker, K. (1974). Methods of Enzymatic Analysis. (New York: Weinheim Academic Press).

Klimyuk, V.I., Carroll, B.J., Thomas, C.M., and Jones, J.D. (1993). Alkali treatment for rapid preparation of plant material for reliable PCR analysis. Plant J. **3,** 493–494.

Kolattukudy, P.E. (1980). Biopolyesters of plants: Cutin and suberin. Science **208,** 990–1000.

Koorneef, M., Hanhart, C.J., and Thiel, F. (1989). A genetic and phenotypic description of *Eceriferum* (*cer*) mutants in *Arabidopsis thaliana*. J. Hered. **80,** 118–122.

Kuhn, D.N., Knauf, M.J., and Stumpf, P.K. (1981). Subcellular localization of acetyl-CoA synthesis in leaf protoplasts of *Spinachia oleracea*. Arch. Biochem. Biophys. **209,** 441–450.

Kursteiner, O., Dupuis, I., and Kuhlemeier, C. (2003). The Pyruvate decarboxylase1 gene of Arabidopsis is required during anoxia but not other environmental stresses. Plant Physiol. **132,** 968–978.

Laemmli, U.K. (1970). Cleavage of structural proteins during the assembly of the head of bacteriophage T4. Nature **227,** 680–685.

Lichtenthaler, H.K. (1987). Chlorophylls and carotenoids: Pigments of photosynthetic membranes. Methods Enzymol. **148,** 350–382.

Liedvogel, B. (1986). Acetyl-CoA and isopentenylpyrophosphate as lipid precursors in plant cells: Biosynthesis and compartmentation. J. Plant Physiol. **124,** 211–222.

Lin, M., Behal, R., and Oliver, D.J. (2003). Disruption of plE2, the gene for the E2 subunit of the plastid pyruvate dehydrogenase complex, in Arabidopsis causes an early embryo lethal phenotype. Plant Mol. Biol. **52,** 865–872.

Masterson, C., Wood, C., and Thomas, D.R. (1990). L-Acetylcarnitine, substrate for chloroplast fatty acid synthesis. Plant Cell Environ. **13,** 755–765.

Mattoo, A.K., and Modi, V.V. (1970). Citrate cleavage enzyme in mango fruit. Biochem. Biophys. Res. Commun. **39,** 895–904.

Millerd, A., and Bonner, J. (1954). Acetate activation and acetoacetate formation in plant systems. Arch. Biochem. Biophys. **49,** 343–355.

Mittler, R. (2002). Oxidative stress, antioxidants and stress tolerance. Trends Plant Sci. **7,** 405–410.

Molina, A., Diaz, I., Vasil, I.K., Carbonero, P., and Garcia-Olmedo, F. (1996). Two cold-inducible genes encoding lipid transfer protein LTP4 from barley show differential responses to bacterial pathogens. Mol. Gen. Genet. **252,** 162–168.

Murashige, T. (1973). Nutrition of plant cells and organs in vitro. In Vitro **9,** 81–85.

Murphy, D.J., and Stumpf, P.K. (1981). The origin of chloroplastic acetyl coenzyme A. Arch. Biochem. Biophys. **212,** 730–739.

Nagpal, P., and Quatrano, R.S. (1999). Isolation and characterization of a cDNA clone from Arabidopsis thaliana with partial sequence similarity to integrins. Gene **230,** 33–40.

Nelson, D.R., and Rinne, R.W. (1975). Citrate cleavage enzyme from developing soybean cotyledons. Plant Physiol. **55,** 69–72.

Nemeth, K., et al. (1998). Pleiotropic control of glucose and hormone responses by PRL1, a nuclear WD protein, in Arabidopsis. Genes Dev. **12,** 3059–3073.

Newman, T., de Bruijn, F.J., Green, P., Keegstra, K., Kende, H., McIntosh, L., Ohlrogge, J., Raikhel, N., Somerville, S., Thomashow, M., Retzel, E., and Somerville, C. (1994). Genes galore: A summary of methods for accessing results from large-scale partial sequencing of anonymous Arabidopsis cDNA clones. Plant Physiol. **106,** 1241–1255.

Nikolau, B.J., Ohlrogge, J.B., and Wurtele, E.S. (2003). Plant biotin-containing carboxylases. Arch. Biochem. Biophys. **414,** 211–222.

Nikolau, B.J., Wurtele, E.S., and Stumpf, P.K. (1985). Use of streptavidin to detect biotin-containing proteins in plants. Anal. Biochem. **149,** 448–453.

Nishitani, K., and Tominaga, R. (1992). Endo-xyloglucan transferase, a novel class of glycosyltransferase that catalyzes transfer of a segment of xyloglucan molecule to another xyloglucan molecule. J. Biol. Chem. **267,** 21058–21064.

op den Camp, R.G., and Kuhlemeier, C. (1997). Aldehyde dehydrogenase in tobacco pollen. Plant Mol. Biol. **35,** 355–365.

Pauly, M., and Scheller, H.V. (2000). O-Acetylation of plant cell wall polysaccharides: Identification and partial characterization of a rhamnogalacturonan O-acetyl-transferase from potato suspension-cultured cells. Planta **210,** 659–667.

Perera, M.A.D.N., Dietrich, C.R., Meeley, R., Schnable, P.S., and Nikolau, B.J. (2003). Dissecting the maize epicuticular wax biosynthetic pathway via the characterization of an extensive collection of glossy mutants. In Advanced Research on Plant Lipids: Proceedings of the 15th International Symposium on Plant Lipids, N. Murata, M. Yamada, I. Nishida, H. Okuyama, J. Sekiya, and H. Wada, eds (Boston: Kluwer Academic Publishers), pp. 225–228.

Pichersky, E., and Gang, D.R. (2000). Genetics and biochemistry of secondary metabolites in plants: An evolutionary perspective. Trends Plant Sci. **5,** 439–445.

Pollard, M., and Stumpf, P.K. (1980). Biosynthesis of C20 and C22 fatty acids by developing seeds of *Limnanthes alba*. Plant Physiol. **66,** 649–655.

Post-Beittenmiller, D. (1996). Biochemistry and molecular biology of wax production in plants. Annu. Rev. Plant Physiol. Plant Mol. Biol. **47,** 405–430.

Qian, H.-R. (2002). Molecular Genetic Studies of Acetyl-CoA Carboxylase and 3-Methylcrotonyl-CoA Carboxylase in Plants. PhD dissertation (Ames, IA: Iowa State University).

Queitsch, C., Sangster, T.A., and Lindquist, S. (2002). Hsp90 as a capacitor of phenotypic variation. Nature **417,** 618–624.

Rabino, I., and Mancinelli, A.L. (1986). Light, temperature, and anthocyanin production. Plant Physiol. **81,** 922–924.

Randall, D.D., Miernyk, J.A., Fang, T.K., Budde, R.J.A., and Schuller, K.A. (1989). Regulation of the pyruvate dehydrogenase complexes in plants. Ann. NY Acad. Sci. **573,** 192–215.

Rangasamy, D., and Ratledge, C. (2000). Compartmentation of ATP: citrate lyase in plants. Plant Physiol. **122,** 1225–1230.

Reid, E.E., Lyttle, C.R., Canvin, D.T., and Dennis, D.T. (1975). Pyruvate dehydrogenase complex activity in proplastids and mitochondria of developing castor bean endosperm. Biochem. Biophys. Res. Commun. **62,** 42–47.

Riesmeier, J.W., Willmitzer, L., and Frommer, W.B. (1994). Evidence for an essential role of the sucrose transporter in phloem loading and assimilate partitioning. EMBO J. **13,** 1–7.

Rodermel, S., Haley, J., Jiang, C.Z., Tsai, C.H., and Bogorad, L. (1996). A mechanism for intergenomic integration: Abundance of ribulose bisphosphate carboxylase small-subunit protein influences the translation of the large-subunit mRNA. Proc. Natl. Acad. Sci. USA **93,** 3881–3885.

Sambrook, J., Fritsch, E.F., and Maniatis, T. (1989). Molecular Cloning: A Laboratory Manual. (Cold Spring Harbor, NY: Cold Spring Harbor Laboratory Press).

Sato, T. (1967). A modified method for lead staining of thin sections. J. Electron Microsc. **17,** 158–159.

Savidge, B., Rounsley, S.D., and Yanofsky, M.F. (1995). Temporal relationship between the transcription of two Arabidopsis MADS box genes and the floral organ identity genes. Plant Cell **7,** 721–733.

Schmid, J., Doerner, P.W., Clouse, S.D., Dixon, R.A., and Lamb, C.J. (1990). Developmental and environmental regulation of a bean chalcone synthase promoter in transgenic tobacco. Plant Cell **2,** 619–631.

Schwender, J., and Ohlrogge, J.B. (2002). Probing in vivo metabolism by stable isotope labeling of storage lipids and proteins in developing *Brassica napus* embryos. Plant Physiol. **130,** 347–361.

Schwender, J., Ohlrogge, J.B., and Shachar-Hill, Y. (2003). A flux model of glycolysis and the oxidative pentosephosphate pathway in developing *Brassica napus* embryos. J. Biol. Chem. **278,** 29442–29453.

Shalit, M., Guterman, I., Volpin, H., Bar, E., Tamari, T., Menda, N., Adam, Z., Zamir, D., Vainstein, A., Weiss, D., Pichersky, E., and Lewinsohn, E. (2003). Volatile ester formation in roses. Identification of an acetyl-coenzyme A geraniol/citronellol acetyltransferase in developing rose petals. Plant Physiol. **131,** 1868–1876.

Shirley, B.W. (1998). Flavonoids in seeds and grains: Physiological function and agronomic importance and the genetics of biosynthesis. Seed Sci. Res. **8,** 415–422.

Shirley, B.W. (2002). Biosynthesis of flavonoids and effects of stress. Curr. Opin. Plant Biol. **5,** 218–223.

Shirley, B.W., Kubasek, W.L., Storz, G., Bruggemann, E., Koornneef, M., Ausubel, F.M., and Goodman, H.M. (1995). Analysis of Arabidopsis mutants deficient in flavonoid biosynthesis. Plant J. **8,** 659–671.

Shockey, J.M., Fulda, M.S., and Browse, J. (2003). Arabidopsis contains a large superfamily of acyl-activating enzymes. Phylogenetic and biochemical analysis reveals a new class of acyl-coenzyme A synthetases. Plant Physiol. **132,** 1065–1076.

Souter, M., Topping, J., Pullen, M., Friml, J., Palme, K., Hackett, R., Grierson, D., and Lindsey, K. (2002). *hydra* mutants of Arabidopsis are defective in sterol profiles and auxin and ethylene signaling. Plant Cell **14,** 1017–1031.

Sperling, P., and Heinz, E. (2003). Plant sphingolipids: Structural diversity, biosynthesis, first genes and functions. Biochim. Biophys. Acta **1632,** 1–15.

Stafford, H. (1995). Metabolism and regulation of phenolics: Gaps in our knowledge. In Phytochemicals and Health, Current Topics in Plant Physiology Series, Vol. 15, D.L. Gustine and H.E. Flores, eds (Rockville, MD: American Society of Plant Physiologists), pp. 15–30.

Stumpf, D.K., and Burris, R.H. (1981). Organic acid contents of soybean: Age and source of nitrogen. Plant Physiol. **68,** 989–991.

Sun, J.M., Spencer, V.A., Chen, H.Y., Li, L., and Davie, J.R. (2003). Measurement of histone acetyltransferase and histone deacetylase activities and kinetics of histone acetylation. Methods **31,** 12–23.

Sunkar, R., Bartels, D., and Kirch, H.H. (2003). Overexpression of a stress-inducible aldehyde dehydrogenase gene from *Arabidopsis*

thaliana in transgenic plants improves stress tolerance. Plant J. **35,** 452–464.

Takeda, Y. (1969). ATP citrate lyase. Seikagaku **41,** 309–324.

Todd, J., Post-Beittenmiller, D., and Jaworski, J.G. (1999). KCS1 encodes a fatty acid elongase 3-ketoacyl-CoA synthase affecting wax biosynthesis in *Arabidopsis thaliana*. Plant J. **17,** 119–130.

von Schaewen, A., Stitt, M., Schmidt, R., Sonnewald, U., and Willmitzer, L. (1990). Expression of a yeast-derived invertase in the cell wall of tobacco and Arabidopsis plants leads to accumulation of carbohydrate and inhibition of photosynthesis and strongly influences growth and phenotype of transgenic tobacco plants. EMBO J. **9,** 3033–3044.

Whitaker, B.D., and Stommel, J.R. (2003). Distribution of hydroxycinnamic acid conjugates in fruit of commercial eggplant (*Solanum melongena* L.) cultivars. J. Agric. Food Chem. **51,** 3448–3454.

Wiedenfeld, H., Pietrosiuk, A., Furmanowa, M., and Roeder, E. (2003). Pyrrolizidine alkaloids from *Lithospermum canescens* Lehm. Z. Naturforsch. C **58,** 173–176.

Wood, C., Jalil, M.N.H., Ariffin, A., Yong, B.C.S., and Thomas, D.R. (1983). Carnitine short chain acyltransferase in pea mitochondria. Planta **158,** 175–178.

Wood, K.V., Bonham, C.C., and Jenks, M.A. (2001). The effect of water on the ion trap analysis of trimethylsilyl derivatives of long-chain fatty acids and alcohols. Rapid Commun. Mass Spectrom. **15,** 873–877.

Wurtele, E.S., Behal, R.H., Cui, X., Ke, J., Johnson, J.L., Lui, F., Nikolau, B.J., Oliver, D.J., and Schnable, P.S. (1999). Molecular biology of acetyl-CoA generation. In Advances in Plant Lipid Research, J. Sanchez, E. Cerda-Olmedo, and E. Martinez-Force, eds (Sevilla, Spain: Secretariado de Publicaciones de la Universidad de Sevilla), pp. 54–56.

Yamaguchi-Shinozaki, K., and Shinozaki, K. (1993). Characterization of the expression of a desiccation-responsive rd29 gene of *Arabidopsis thaliana* and analysis of its promoter in transgenic plants. Mol. Gen. Genet. **236,** 331–340.

Yoshiba, Y., Kiyosue, T., Katagiri, T., Ueda, H., Mizoguchi, T., Yamaguchi-Shinozaki, K., Wada, K., Harada, Y., and Shinozaki, K. (1995). Correlation between the induction of a gene for delta 1-pyrroline-5-carboxylate synthetase and the accumulation of proline in *Arabidopsis thaliana* under osmotic stress. Plant J. **7,** 751–760.

Zeeman, S.C., Northrop, F., Smith, A.M., and Rees, T. (1998). A starch-accumulating mutant of *Arabidopsis thaliana* deficient in a chloroplastic starch-hydrolysing enzyme. Plant J. **15,** 357–365.